CANCER

CECR2 drives breast cancer metastasis by promoting NF-κB signaling and macrophage-mediated immune suppression

Meiling Zhang[1], Zongzhi Z. Liu[1]†, Keisuke Aoshima[1,2], Wesley L. Cai[1,3], Hongyin Sun[4], Tianrui Xu[4], Yangyi Zhang[1,4], Yongyan An[1], Jocelyn F. Chen[1], Lok Hei Chan[1], Asako Aoshima[1], Sabine M. Lang[1], Zhenwei Tang[4], Xuanlin Che[4], Yao Li[1], Sara J. Rutter[1]‡, Veerle Bossuyt[1]§, Xiang Chen[4], Jon S. Morrow[1,5], Lajos Pusztai[5,6], David L. Rimm[1,5], Mingzhu Yin[1,4]*, Qin Yan[1,5,7,8]*

Metastasis is the major cause of cancer-related deaths due to the lack of effective therapies. Emerging evidence suggests that certain epigenetic and transcriptional regulators drive cancer metastasis and could be targeted for metastasis treatment. To identify epigenetic regulators of breast cancer metastasis, we profiled the transcriptomes of matched pairs of primary breast tumors and metastases from human patients. We found that distant metastases are more immune inert with increased M2 macrophages compared to their matched primary tumors. The acetyl-lysine reader, cat eye syndrome chromosome region candidate 2 (CECR2), was the top up-regulated epigenetic regulator in metastases associated with an increased abundance of M2 macrophages and worse metastasis-free survival. CECR2 was required for breast cancer metastasis in multiple mouse models, with more profound effect in the immunocompetent setting. Mechanistically, the nuclear factor κB (NF-κB) family member v-rel avian reticuloendotheliosis viral oncogene homolog A (RELA) recruits CECR2 to increase chromatin accessibility and activate the expression of their target genes. These target genes include multiple metastasis-promoting genes, such as *TNC*, *MMP2*, and *VEGFA*, and cytokine genes *CSF1* and *CXCL1*, which are critical for immunosuppression at metastatic sites. Consistent with these results, pharmacological inhibition of CECR2 bromodomain impeded NF-κB–mediated immune suppression by macrophages and inhibited breast cancer metastasis. These results reveal that targeting CECR2 may be a strategy to treat metastatic breast cancer.

INTRODUCTION

Breast cancer is the most common cancer among women worldwide and the second leading cause of cancer-related deaths in the United States (*1*, *2*). The major cause of cancer-related deaths is metastasis to distal organs, including lung, brain, and bone (*3*, *4*). Patients with metastatic breast cancer respond poorly to current therapies (*2*). Thus, there is an urgent need to identify additional therapeutic targets for metastatic breast cancers.

Cancer metastasis is a multistep process that involves dynamic cross-talk between tumor cells and other cells in the tumor microenvironment (*4*–*6*). As one of the major immune cell populations in the breast tumor microenvironment, tumor-associated macrophages (TAMs) promote breast tumor growth and metastasis and are associated with poor survival of breast cancer patients (*7*–*9*). Macrophages can be polarized into either classically activated M1 macrophages with a proinflammatory role or alternatively activated M2 macrophages that are immunosuppressive (*10*, *11*). Although different macrophage subpopulations have been observed in the tumor microenvironment, TAMs commonly express CD68 receptor and resemble M2 macrophages (*12*–*14*). These macrophages promote tumor progression and metastasis by stimulating angiogenesis, migration, invasion, extravasation, and growth of cancer cells and suppress antitumor immunity (*15*, *16*). TAMs located in distal metastatic sites express different receptors from the TAMs interacting with the primary breast tumor (*16*, *17*). Therefore, a better understanding of how TAMs are regulated in metastatic progression will facilitate the development of therapeutic intervention against cancer metastasis (*16*, *18*).

Epigenetic aberrations play critical roles in driving breast cancer metastasis and may be reversibly regulated by targeting epigenetic regulators (*4*, *19*–*23*). Cat eye syndrome chromosome region candidate 2 (CECR2) is an epigenetic factor with a bromodomain that recognizes acetylated lysine residues. CECR2 was shown to play critical roles in DNA damage responses (*24*), neurulation (*25*), and spermatogenesis (*26*). It was reported that CECR2 participates in chromatin remodeling by interacting with sucrose nonfermenting 2 like and homolog (SNF2L and SNF2H, respectively) (*25*, *26*). The bromodomain of CECR2 was predicted to be highly druggable (*27*). Two highly potent and specific CECR2 inhibitors, GNE-886 and NVS-CECR2-1, have been developed by Genentech (*28*) and the joint effort of Structural Genomics Consortium (SGC) and Novartis (*29*), respectively. However, the specific functions of CECR2 in cancer, especially in metastasis, remain unclear.

[1]Department of Pathology, Yale School of Medicine, New Haven, CT 06520, USA. [2]Laboratory of Comparative Pathology, Department of Veterinary Clinical Sciences, Faculty of Veterinary Medicine, Hokkaido University, Sapporo 060-0818, Japan. [3]Hillman Cancer Center, University of Pittsburgh Medical Center, Pittsburgh, PA 15232, USA. [4]Department of Dermatology, Hunan Engineering Research Center of Skin Health and Disease, Hunan Key Laboratory of Skin Cancer and Psoriasis, Xiangya Hospital, Central South University, Changsha, Hunan 410008, China. [5]Yale Cancer Center, Yale School of Medicine, New Haven, CT 06520, USA. [6]Breast Medical Oncology, Yale Cancer Center, Yale University, New Haven, CT 06520, USA. [7]Yale Stem Cell Center, Yale School of Medicine, New Haven, CT 06520, USA. [8]Yale Center for Immuno-Oncology, Yale School of Medicine, New Haven, CT 06520, USA.
*Corresponding author. Email: qin.yan@yale.edu (Q.Y.); yinmingzhu2008@126.com (M.Y.)
†Present address: Department of R&D Bioinformatics, Sema4 Inc., Stamford, CT 06902, USA.
‡Present address: Methodist Pathology Center, Methodist Hospital, 8303 Dodge Street, Omaha, NE 68114, USA.
§Present address: Department of Pathology, Massachusetts General Hospital, Harvard Medical School, Boston, MA 02114, USA.

Here, we identify CECR2 as an epigenetic driver of breast cancer metastasis and a potential therapeutic target for metastatic breast cancer. By profiling the transcriptomes of 13 matched pairs of primary and metastatic breast tumors, we show that a variety of immune cell types and immune-oncology targets are altered in metastases. Metastatic samples exhibit increased ratio of M2 macrophages, which are correlated with higher CECR2 expression. CECR2 depletion inhibits recruitment and polarization of TAMs and results in a marked decrease of metastasis in multiple mouse breast cancer models. Mechanistic studies show that CECR2 forms a complex with v-rel avian reticuloendotheliosis viral oncogene homolog A (RELA) through its bromodomain to increase chromatin accessibility and modulate the expression of epithelial-mesenchymal transition (EMT) genes and nuclear factor κB (NF-κB) target genes, including *CSF1* and *CXCL1*. Consistent with these results, pharmacological inhibition of CECR2 suppresses NF-κB target gene expression, M2 macrophage polarization, and breast cancer metastasis. Together, these findings suggest that CECR2 plays a key role in breast cancer metastasis and nominate it as a promising therapeutic target against metastatic diseases.

RESULTS

Distal metastases are more immune inert with increased M2 macrophages than primary breast tumors

The tumor microenvironment plays key roles in shaping cancer metastasis and in determining treatment responses (*30*). By analyzing 730 immune-related genes using Nanostring technology, we showed recently that metastatic breast cancers have a more immunologically inert tumor microenvironment than primary tumors (*31*). However, it is poorly understood how tumor cells contribute to the establishment of this tumor microenvironment. To characterize the differences in immune microenvironment more extensively and to identify regulators of tumor immune microenvironment and drivers of metastasis, we compared transcriptomes of 13 pairs of matched primary and distant metastatic breast cancer tumor samples using RNA sequencing (RNA-seq) analysis (Fig. 1A). The median age of these patients was 51 years, and their median overall survival time was 4 years (data file S1). Six patients had estrogen receptor–positive (ER^+) tumors, and seven patients had ER-negative (ER^-) tumors. Tumor metastases for these patients were found in different locations, including ovary, lung, brain, liver, spine, esophagus, skin, stomach, fallopian tubes, and soft tissue. Hierarchical clustering analysis revealed that all tumors from ER^+ patients were clustered into one group, whereas most of the ER^- tumors clustered into another group (fig. S1A) (*32*). We found that the gene expression profiles of primary and metastatic tumors from the same patient tend to cluster together, despite their divergent locations, as reported previously (*32*). We found 930 differentially expressed genes, among which 627 genes were down-regulated and 303 genes were up-regulated in the matched distant metastases versus the primary tumors (data file S2).

Gene set enrichment analysis (GSEA) showed that several immune-related pathways were down-regulated in metastatic samples, including interferon-γ (IFN-γ) responses, IFN-α responses, and inflammatory responses (fig. S1B). Consistently, most immune-related genes were down-regulated in the metastases compared to the matched primary tumors, especially the genes involved in macrophage function and T cell activation (Fig. 1B). Genes encoding antitumor immune response and activation markers, including programmed cell death ligand 1 (*PD-L1*), granzyme B (*GZMB*), and perforin (*PRF1*), were all decreased in the metastastic tumor microenvironment (Fig. 1C). Genes associated with inflammatory macrophages, such as *CD68* and toll-like receptor 2 (*TLR2*), were down-regulated, whereas vascular endothelial growth factor A (*VEGFA*), which contributes to cancer metastasis and M2 macrophage polarization, was up-regulated in the metastatic tumor microenvironment (Fig. 1C). Consistently, GZMB protein abundance decreased in the metastases (fig. S1, C and D). We also found that 20 of 29 immuno-oncology target genes were down-regulated in metastatic tumors compared to their matched primary tumors, in which 4 genes (*TLR1*, *TLR8*, *TLR2*, and *TLR7*) were associated with macrophage functions (*33*, *34*), 4 genes (*CCR4*, *CXCL12*, *CXCR4*, and *CCR2*) were associated with immune cell trafficking, and 3 genes [cytotoxic T lymphocyte–associated protein 4 (*CTLA-4*), *CD27*, and *CD274/PD-L1*] were involved in immune checkpoint function (Fig. 1D and data file S3).

To understand the difference of the immune cell composition in matched primary and metastatic tumor microenvironment, we analyzed the RNA-seq data using CIBERSORTx (*35*). The major components of immune cells from CIBERSORTx analysis were macrophages, $CD4^+$ T cells, and B cells in tumor microenvironment (data file S4). Intriguingly, the M1 macrophage population significantly decreased, and the ratio of M2 macrophages to total macrophages increased in metastasis tumors ($P < 0.05$; Fig. 1E and fig. S1E). However, the proportion of total macrophages showed no difference between primary tumors and matched metastases, nor did $CD8^+$ and $CD4^+$ T cells, natural killer (NK) cells, dendritic cells, or neutrophils (fig. S1, F to K). These results indicate that the population variation of macrophages, especially the M2 ratio, is the major immunological difference between the primary and metastatic breast cancer tumor microenvironment in our dataset.

CECR2 expression is correlated with breast cancer metastasis

Epigenetic and transcriptional changes have been implicated in metastatic progression (*4*). Thus, we focused our attention on epigenetic regulators that were altered in the metastatic samples compared with matched primary ones. To this end, we compared the list of differentially expressed genes with the list of genes involved in epigenetic regulation that we compiled (data file S5) by combining the epigenetic gene lists in the literature (*36*, *37*) and at the SGC website. Among the 24 significantly deregulated epigenetic genes with fold change of more than 1.5 ($P < 0.05$; Fig. 2, A and B, and data file S6), *PPARGC1A*, an up-regulated gene in metastases that encodes peroxisome proliferator–activated receptor gamma coactivator–1α (PGC-1α), was reported to promote breast cancer metastasis (*38*). We found several additional potential epigenetic or transcriptional regulators of breast cancer metastasis, including CECR2, forkhead box protein (FOXP) family proteins, nuclear body proteins, DNA methylation regulators, and positive regulatory (PR) domain proteins. The expression of these genes was not clustered by ER or human epidermal growth factor receptor 2 (HER2) status but by their primary tumor or metastasis status (Fig. 2B), implying their general roles in affecting metastatic capability across breast cancer subtypes.

The transcriptomes of primary and metastatic breast cancer tumors indicated that metastatic tumor microenvironments were more immunologically inert in breast cancer (Fig. 1). To investigate how epigenetic change regulated the immune microenvironment during breast cancer metastasis, we analyzed the correlation of the M2 macrophage ratio with the expression of each dysregulated epigenetic

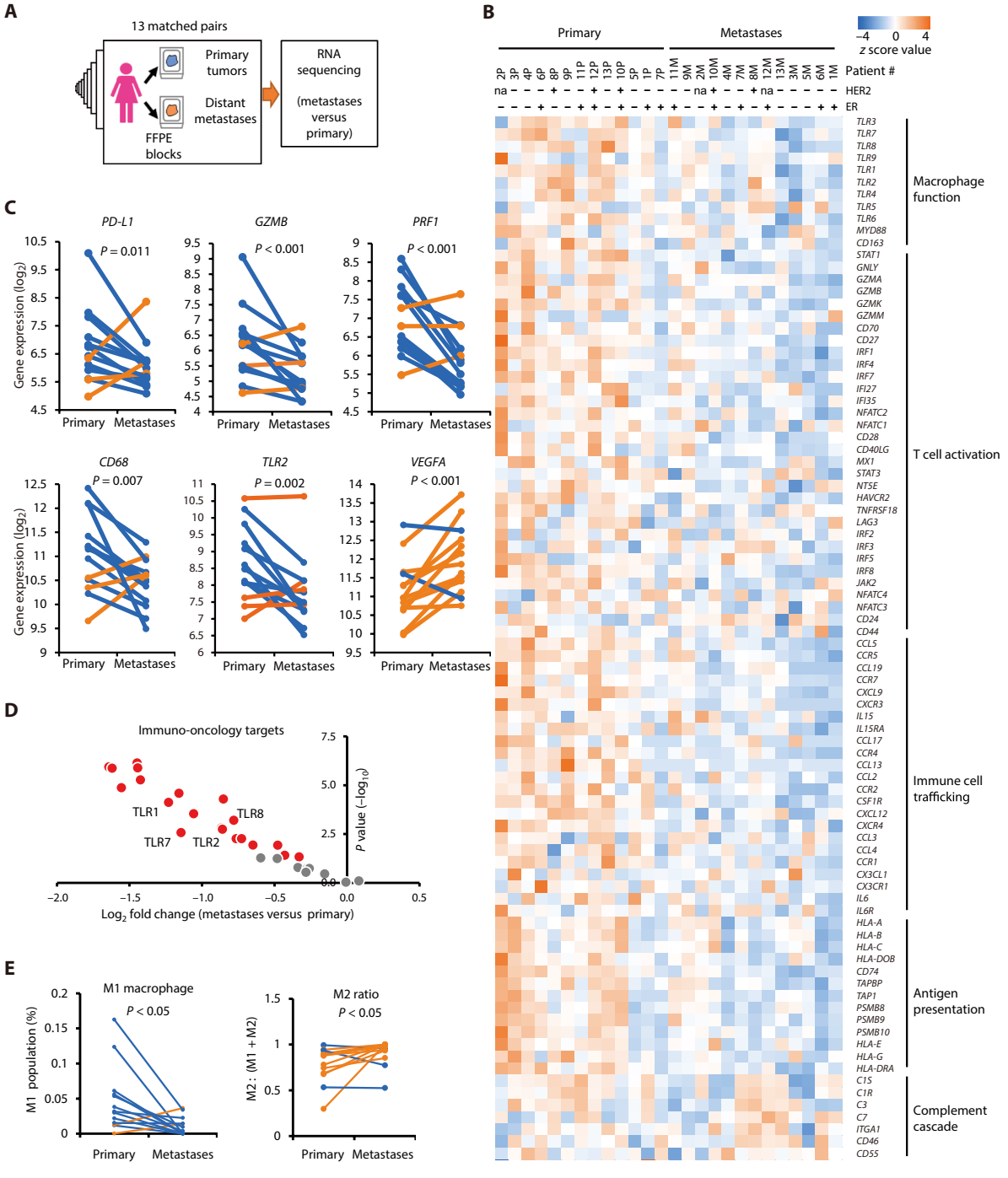

Fig. 1. Immune-related gene signatures differ between metastatic and primary breast cancer. (**A**) Matched primary tumors and distal metastases from 13 breast cancer patients were collected, and deregulated genes were analyzed by comparing distal metastases with matched primary tumors using RNA sequencing (RNA-seq) analysis. FFPE, formalin-fixed, paraffin embedded. (**B**) A heatmap shows the expression of representative immune genes of tolerance mechanisms in 13 pairs of primary and matched metastatic breast cancer tumor samples. HER2 and ER status is shown; "+" means that the status is positive, and "−" means that the status is negative. na, not assessed (means the absence of patient information). (**C**) Tumor-infiltrating lymphocyte– and macrophage-related gene expression was compared in matched pairs of metastatic and primary breast tumor samples. Orange lines mark the samples with increased expression in metastases, and blue lines mark the ones with decreased expression. (**D**) Volcano plot of down-regulated immune-oncology targets for matched metastatic samples compared with primary breast tumors. Red dots denote the significantly changed targets. (**E**) RNA-seq data of matched primary tumor and distal metastases from 13 breast cancer patients were analyzed by CIBERSORTx, and immune cell composition of complex tissues was characterized from their gene expression profiles. Populations of M1 macrophages and the ratio of M2 macrophages to the total macrophages in primary and matched metastatic breast cancer samples are shown. Orange lines mark the samples with increased numbers in metastases, and blue lines mark the ones with decreased numbers. The *P* values were obtained using DESeq2 analysis of the counts (C and D) and Wilcoxon signed-rank test (E).

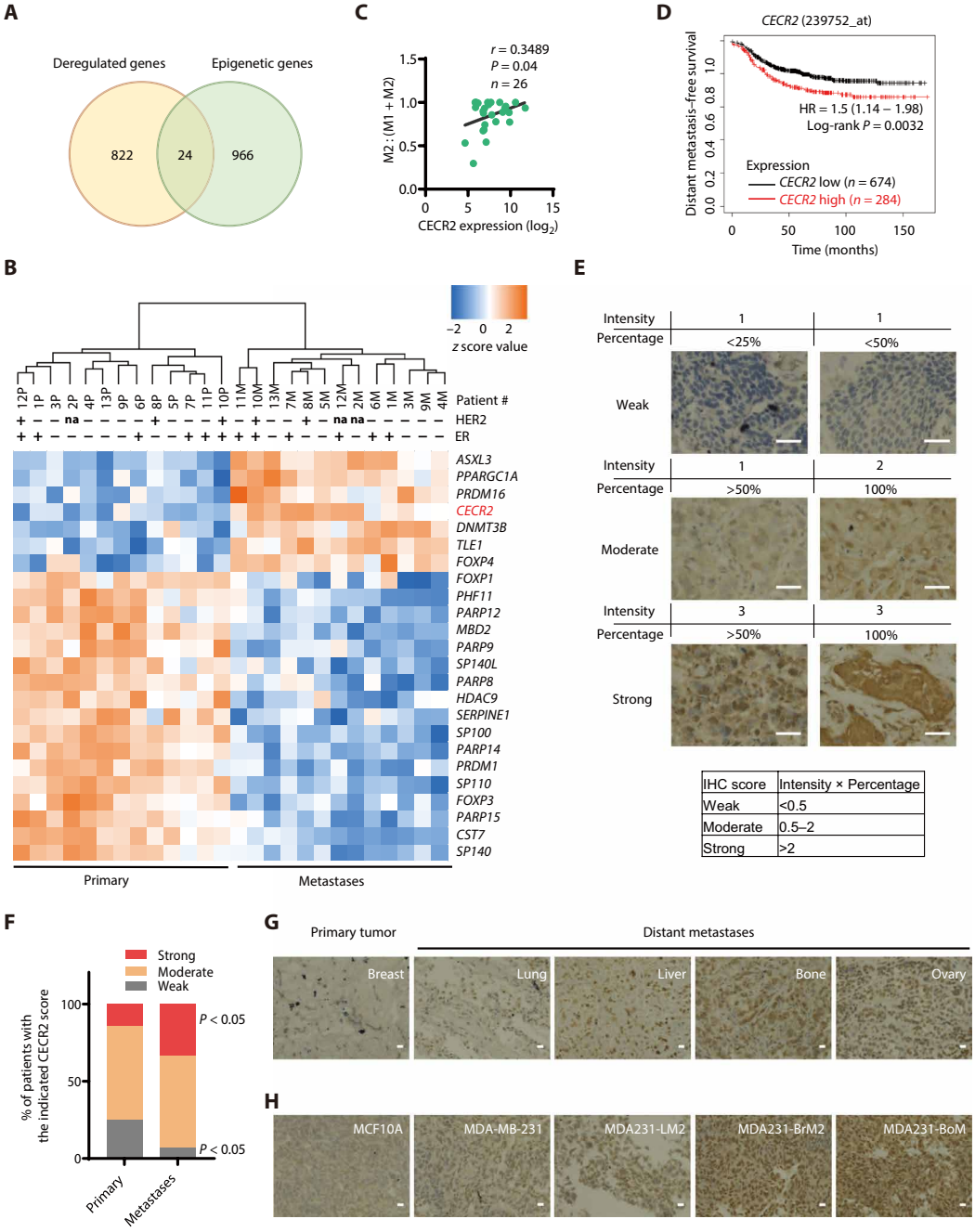

Fig. 2. CECR2 is highly expressed in breast cancer metastases and correlates with M2 macrophage abundance. (**A**) The Venn diagram shows deregulated epigenetic genes with significantly changed mRNA expression (fold change > 1.5) by RNA-seq in metastatic samples compared to primary samples. (**B**) The heatmap shows the significantly deregulated epigenetic genes. *CECR2* is highlighted in red. HER2 and ER status is shown; + means that the status is positive, and – means that the status is negative. (**C**) The plot shows the correlation between M2 ratios and *CECR2* expression. RNA-seq data of matched primary tumor and distal metastases from 13 breast cancer patients were analyzed by CIBERSORTx, and immune cell composition of complex tissues was characterized from their gene expression profiles. Pearson correlation coefficient and one-tailed probability *P* value are shown. (**D**) Kaplan-Meier analysis shows the association of *CECR2* mRNA abundance with distant metastasis–free survival of breast cancer patients using the best cutoff. The cutoff value is 123 in the expression range of 2 to 1738. The hazard ratio (HR) and log-rank *P* values are shown. (**E**) CECR2 immunohistochemical (IHC) staining for a tumor tissue microarray with 59 pairs of matched primary and metastatic breast cancer samples. Representative figures are shown. Scale bars, 100 μm. (**F**) CECR2 IHC scores were quantified by multiplying the intensity of the signal and the percentage of positive cells. The IHC staining of tumors was scored as weak (score < 0.5), moderate (score between 0.5 and 2), and strong (score > 2). Percentage of patient samples with strong CECR2 abundance in metastatic tumors versus that in primary tumor, $P < 0.05$. Percentage of samples with weak CECR2 abundance in metastatic tumors versus that in primary tumor, $P < 0.05$. The *P* values of unpaired two-tailed Student's *t* test are shown. (**G**) CECR2 IHC staining of matched primary and multiple distant metastasis samples for a single patient with breast cancer. Scale bars, 100 μm. (**H**) CECR2 IHC staining of MCF10A and MDA-MB-231 and its metastatic derivatives (MDA231-LM2, MDA231-BrM2, and MDA231-BoM). Scale bars, 100 μm.

factor. Among 13 epigenetic factors correlated with the ratio of M2 macrophage, *CECR2* was a top up-regulated gene in metastases associated with poor metastasis-free survival (Fig. 2C and data file S7). Kaplan-Meier analysis (*39*) showed that high *CECR2* mRNA concentrations were associated with poor distant metastasis–free survival for patients with breast cancer overall and in ER^+, $HER2^+$, and ER^- breast cancer subtypes (Fig. 2D, fig. S2A, and data file S7). Similar results were found in gastric and ovarian cancer cohorts (fig. S2, B and C).

Here, we focused on CECR2 because it is an attractive targetable epigenetic regulator of breast cancer metastasis. Increased *CECR2* mRNA concentrations in distant metastases were confirmed by quantitative reverse transcription polymerase chain reaction (RT-qPCR) assays (fig. S2D). We further examined CECR2 protein abundance by immunohistochemical (IHC) staining of a tissue microarray composed of 59 pairs of matched human primary tumors and distant metastases [data file S8; expanded from previously described (*31*)]. Two pathologists independently evaluated CECR2 expression by IHC scores (stain intensity score multiplied by the percentage of positive tumor cells) and found that higher CECR2 protein abundance was more frequently observed in cancer cells in distant metastases than in primary tumors (33.3% versus 14.1%) (Fig. 2, E and F, and data file S8). To characterize the relationship of CECR2 expression with the location of metastases, we performed IHC staining with breast cancer samples taken from one patient with multiple metastatic sites, including lung, liver, bone, and ovary. We found that all the metastatic samples have higher expression of CECR2, with the highest expression in the bone and ovary (Fig. 2G). We also compared CECR2 expression in immortalized MCF10A breast epithelial cells, triple-negative MDA-MB-231 breast cancer cells (MDA231), and MDA231-derived metastatic cell lines, including MDA231-LM2 (LM2), MDA231-BrM2 (BrM2), and MDA231-BoM (BoM) cells. These three MDA231 metastatic cell lines were derived by in vivo selection, with increased metastatic activity to the lungs, brain, and bones, respectively, compared with their parental cells (*40*–*42*). CECR2 protein was expressed at a higher degree in MDA231 cells than in MCF10A cells (Fig. 2H). All three MDA231 derivatives have increased CECR2 protein abundance compared with the parental MDA231 cells (Fig. 2H). Together, CECR2 abundance is correlated with increased metastatic potential.

CECR2 is critical for migration, invasion, and metastasis

To dissect the roles of CECR2 in metastasis, we first generated polyclonal LM2 cell lines with stable *CECR2* knockout (*CECR2* sg) or nontargeting control using the clustered regularly interspaced short palindromic repeats (CRISPR)–CRISPR-associated protein 9 (Cas9) system (Fig. 3A) (*43*). Firefly luciferase was engineered into these LM2 cells to monitor the metastasis signal in vivo by a live imaging system (*41*). Depletion of CECR2 has no effect on cell proliferation in both WST1 cell proliferation and colony formation assays (fig. S3, A and B). Migration and invasion through tissue basement membrane are key steps of metastasis. Using scratch assays, transwell migration assays and invasion assays, we found that CECR2 depletion decreased the migration and invasion capability of LM2 cells by two- to threefold, suggesting that CECR2 has prometastatic functions (Fig. 3, B and C, and fig. S3C).

To determine the roles of CECR2 in metastasis in vivo, LM2 cells with stable *CECR2* knockout or control were injected into the tail veins of athymic nude mice. We found that *CECR2* knockout led to about fivefold decrease in the lung colonization capability of LM2 cells and extended the survival of tumor-bearing mice using bioluminescence signal as the end point (Fig. 3, D and E, and fig. S3D). Consistently, histological analysis of mouse lungs showed that *CECR2* knockout LM2 cells formed about 50% of metastatic lesions as control cells (Fig. 3, F and G, and fig. S3E).

We next extended our studies using a 4T1 mouse triple-negative breast cancer cell line with stable *Cecr2* knockout and stable expression of firefly luciferase (fig. S4, A and B). Consistent with the results in LM2 cells, *Cecr2* deletion decreased cell invasion but not tumor cell proliferation (fig. S4, C to F). Furthermore, CECR2 depletion in 4T1 cells suppressed their metastatic potential to the lungs by about sixfold and extended the survival of tumor-bearing BALB/c nude mice using bioluminescence signal as the end point (fig. S4, G to I). Histological analysis of mouse lungs showed that *Cecr2* knockout 4T1 cells formed about 50% of metastatic lesions as control cells (figs. S3E and S4J).

We found that metastatic sites have different tumor immune microenvironments from primary tumors (Fig. 1) (*31*); thus, we examined the effects of CECR2 loss in an immunocompetent setting. To eliminate the off-target effect of *Cecr2* single-guide RNA, we also restored CECR2 expression in *Cecr2* knockout 4T1 cells using human *CECR2* (fig. S4K). We then injected these cells into wild-type (WT) BALB/c mice through the tail vein and monitored their ability to colonize the lungs. *Cecr2* knockout led to about 38-fold decrease of lung metastasis and extended the survival of tumor-bearing mice using bioluminescence signal as the end point, and restored expression of CECR2 almost completely rescued the phenotype (Fig. 3, H to J, and fig. S4, L and M). Of note, suppression of metastasis by *Cecr2* loss in immunocompetent mice (38-fold) is more profound than that in immunodeficient mice (6-fold), suggesting that tumor immune microenvironment contributes to this difference. Consistent with the role of CECR2 in distal metastasis, CECR2 depletion in 4T1 cells did not affect their tumor growth rate in mammary fat pads of immunocompetent mice but decreased spontaneous lung metastasis by 40% (fig. S4, N and O).

To investigate whether CECR2 loss affects tumor metastasis to other organs, we injected 4T1 control and *Cecr2* knockout cells into the left ventricle of WT BALB/c mice and monitored their ability to metastasize (Fig. 3K). We found that 4T1 tumors metastasize to multiple organs, including brain, liver, and bone. We detected less metastatic signal in mice bearing *Cecr2* knockout cells (17-fold decrease) compared to control cells by measuring the whole-body in vivo tumor bioluminescence signal (Fig. 3L). We further measured the ex vivo tumor bioluminescence signal in the brain, bone, and liver at the end point and found that CECR2 depletion reduced metastasis to the brain, bone, and liver by 46-, 26-, and 4287-fold, respectively (Fig. 3, M to P).

CECR2 activates the NF-κB pathway and EMT pathway

To investigate the underlying molecular mechanisms by which CECR2 modulates breast cancer metastasis, we examined the transcriptome changes in LM2 cells after *CECR2* knockout using RNA-seq analysis. We observed 1051 up-regulated and 1440 down-regulated genes in LM2 cells with *CECR2* sg1 (data file S9). Similarly, there were 1708 up-regulated and 1772 down-regulated genes in LM2 cells with *CECR2* sg2 (data file S10). GSEA revealed eight shared down-regulated pathways and two shared up-regulated pathways by *CECR2* sg1 and sg2 (Fig. 4, A and B; fig. S5, A and B; and data files S11 to S14). The

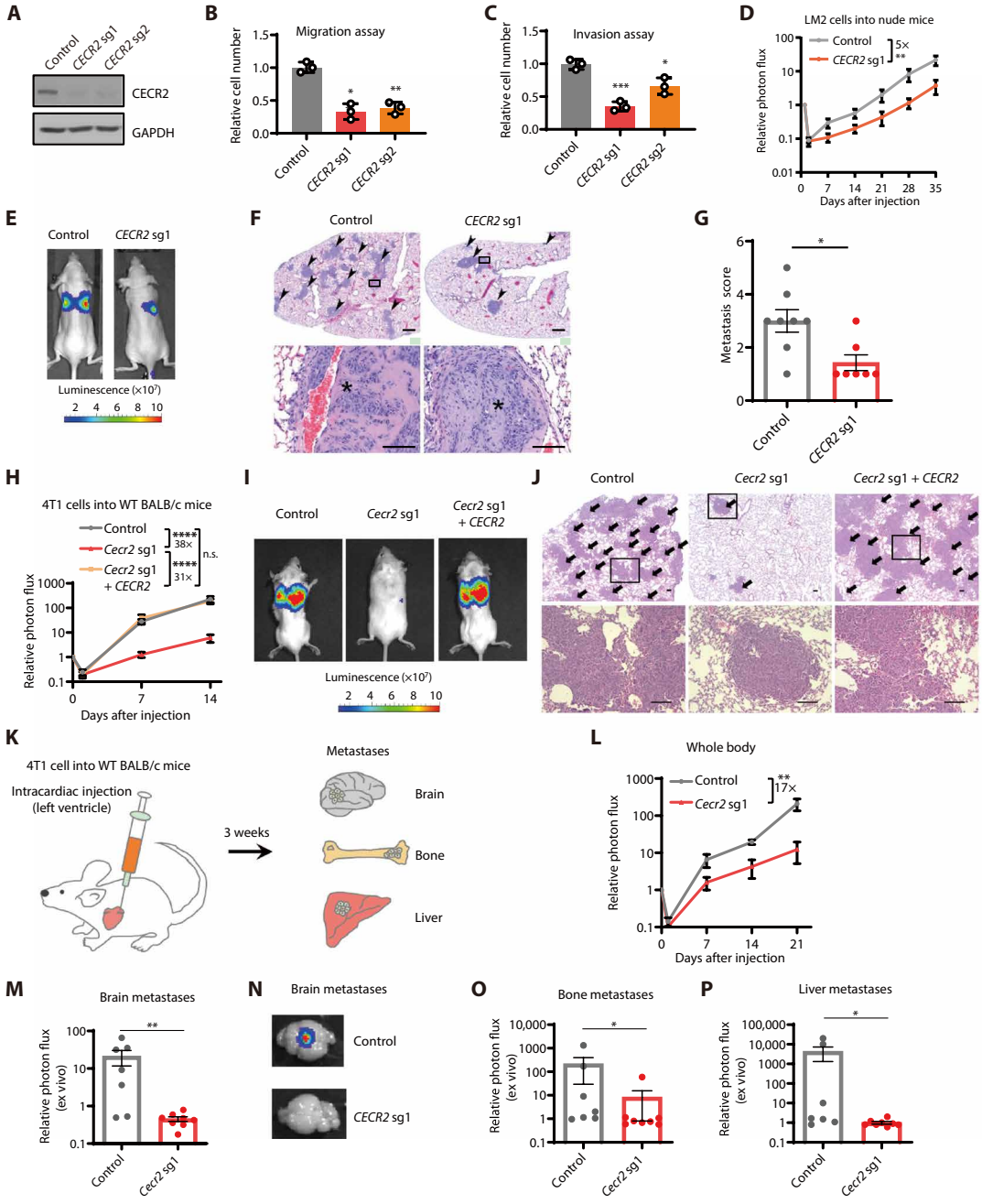

Fig. 3. CECR2 is required for migration, invasion, and metastasis. (**A**) Western blot analysis of control and *CECR2* knockout (sg1 and sg2) LM2 cells. GAPDH, glyceraldehyde-3-phosphate dehydrogenase. (**B** and **C**) Transwell migration (B) and invasion (C) assays were used to compare *CECR2* knockout and control LM2 cells. (**D**) Normalized bioluminescence signals for lung metastases in athymic nude mice after tail vein injection of control ($n = 8$) or *CECR2* knockout LM2 cells ($n = 7$). Fold change at day 35 is shown. (**E**) Representative bioluminescence images of mice in (D) at week 5. (**F**) H&E staining of the lungs from mice in (D) at week 5. Scale bars, 500 μm (top) and 100 μm (bottom). Arrowheads indicate metastatic tumors, and asterisks indicate vascular invasion of large tumor foci. (**G**) Metastatic tumors were scored on the basis of the percentage of tumors in the lungs with the parameters described in fig. S3E. (**H**) Normalized bioluminescence signal for lung metastases in immunocompetent wild-type (WT) BALB/c mice after tail vein injection of control 4T1 ($n = 10$), *Cecr2* knockout 4T1 ($n = 10$), and *Cecr2* knockout 4T1 with *CECR2* reconstituted expression ($n = 10$). Fold change at day 14 is shown. (**I**) Representative bioluminescence images of mice in (H) at week 2. (**J**) H&E staining for lungs from mice in (H) at week 2. Scale bars, 200 μm. Arrows indicate metastatic tumors. (**K**) Schematic of metastasis assay using intracardiac (IC) injection. Mice were monitored for metastasis to the whole body, especially in the brain, bone, and liver. (**L** to **P**) Normalized in vivo bioluminescence signals of whole-body metastases (L) as well as ex vivo bioluminescence signals and representative pictures of brain metastases (M and N) and ex vivo bioluminescence signals of bone metastases (O) and liver metastasis (P) in WT BALB/c mice after IC injection of control ($n = 7$) or *Cecr2* knockout (sg1) ($n = 8$) 4T1 cells. Fold change at day 21 is shown in (L). The *P* values of unpaired two-tailed Student's *t* test (B and C) and Mann-Whitney test (D, G, H, L, M, O, and P) are shown. *$P < 0.05$; **$P < 0.01$; ***$P < 0.001$; ****$P < 0.0001$; n.s., not significant. Representative data from triplicate experiments are shown (B and C), and data are presented as mean ± SEM.

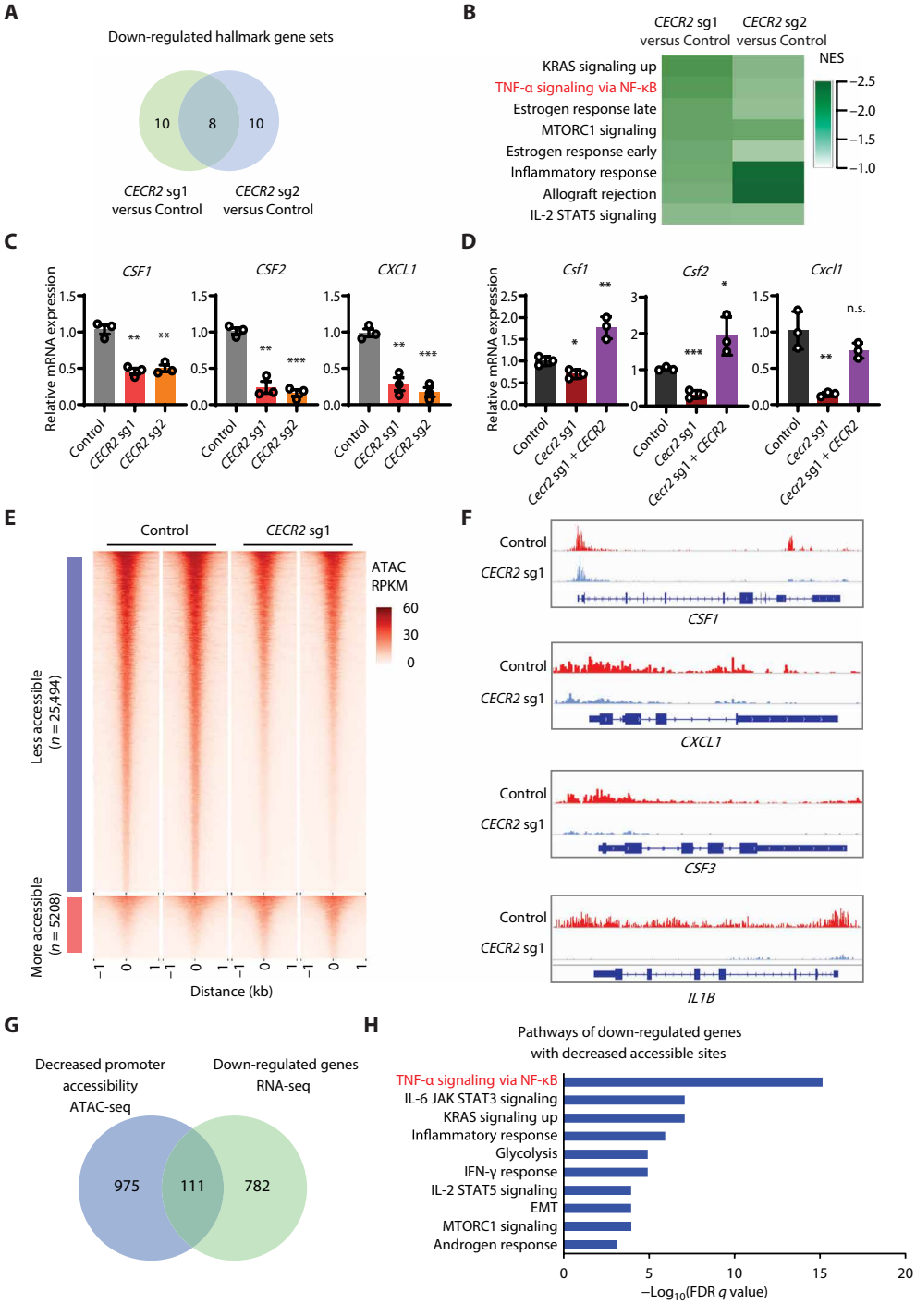

Fig. 4. CECR2 depletion down-regulates NF-κB response genes. (**A** and **B**) GSEA comparing transcriptomes of *CECR2* knockout (*CECR2* sg1 and *CECR2* sg2) with control LM2 cells. The Venn diagram (A) shows the number of shared down-regulated hallmark pathways, and (B) the heatmap shows the eight shared down-regulated hallmark pathways. NES, normalized enrichment score. (**C**) RT-qPCR analysis of *CSF1*, *CSF2*, and *CXCL1* expression in control and *CECR2* knockout LM2 cells. (**D**) RT-qPCR analysis of *Csf1*, *Csf2*, and *Cxcl1* expression in control 4T1, *Cecr2* knockout 4T1, and *Cecr2* knockout 4T1 with *CECR2* reconstituted expression. (**E**) The heatmap shows ATAC-seq peaks for chromatin-accessible sites decreased (top) or increased (bottom) by CECR2 depletion, with the aggregated reads within 1 kb of the center of differentially accessible regions. RPKM, Reads Per Kilobase of transcript, per Million mapped reads. (**F**) ATAC-seq signals around *CSF1*, *CXCL1*, *CSF3*, and *IL1B* genes showing promoter or putative enhancer regions that are less accessible in *CECR2*-deficient (sg1) LM2 cells. (**G**) The Venn diagram shows genes that are down-regulated and with decreased ATAC-seq signals in the promoter after CECR2 depletion in LM2 cells. All of the genes are significantly changed with the cutoff of adjusted $P < 0.05$ and fold change > 1.2. (**H**) Top 10 hallmark pathways enriched for down-regulated genes with decreased ATAC-seq signaling in the promoter after CECR2 depletion in LM2 cells. The *P* values of unpaired two-tailed Student's *t* test (C and D) are shown. $^{*}P < 0.05$; $^{**}P < 0.01$; $^{***}P < 0.001$. Representative data from triplicate experiments are shown, and data are presented as mean ± SEM. FDR, false discovery rate.

down-regulated pathways include tumor necrosis factor–α (TNF-α) signaling by NF-κB, inflammatory response, Kirsten rat sarcoma virus (KRAS) signaling, and estrogen response (Fig. 4B). Gene ontology (GO) analysis also revealed down-regulation of EMT and TNF-α signaling by NF-κB pathway genes after CECR2 depletion (fig. S5, C and D). Most NF-κB response genes and EMT genes were suppressed by *CECR2* knockout, including cytokine genes *CSF1*, *CSF2*, *CSF3*, *CXCL1*, *IL1B*, and *IL6* (fig. S5, E and F). The regulation of selected NF-κB response genes by CECR2 was confirmed by RT-qPCR or Western blot analyses (Fig. 4, C and D, and fig. S5, G and H). *CECR2* expression was not affected by cytokines that are known to activate NF-κB signaling, including interleukin-1β (IL-1β), TNF-α, and IL-6 (fig. S5, I and J).

CECR2 was reported to form chromatin remodeling complexes with SNF2L or SNF2H; thus, it may affect chromatin accessibility (*25*, *26*). We therefore performed assay for transposase-accessible chromatin using sequencing (ATAC-seq) of *CECR2* knockout and control LM2 cells. *CECR2* knockout decreased chromatin accessibility globally, with far more genomic loci with decreased accessibility (n = 25,494) than with increased accessibility (n = 5208) (Fig. 4E and fig. S5K). The loci with decreased chromatin accessibility include promoters or putative enhancers of NF-κB response genes, *CSF1*, *CXCL1*, *CSF3*, and *IL1B* (Fig. 4F), all of which were down-regulated upon CECR2 depletion. We then performed integrative analysis of ATAC-seq and RNA-seq datasets. CECR2 depletion resulted in 111 down-regulated genes with decreased promoter-proximal ATAC-seq peaks (Fig. 4G and data file S15) and only 38 up-regulated genes with increased chromatin accessibility at the promoters (fig. S5L and data file S16). GO analysis indicated that the down-regulated genes with decreased chromatin accessibility upon *CECR2* loss were enriched for genes in the NF-κB pathway and inflammatory response (Fig. 4H and data file S17). Therefore, these data indicate that *CECR2* knockout attenuates chromatin accessibility to down-regulate target genes in the NF-κB pathway.

CECR2 binds to acetylated RELA to activate NF-κB response genes

We then asked whether CECR2 loss affects transcription factors that control the expression of NF-κB–targeted genes. *CECR2* knockout did not change the protein abundance of NF-κB family members, including RELA/p65, p50, RELB, p52, and cREL in the cytosol and nucleus (fig. S6A). Coimmunoprecipitation experiments showed that CECR2 interacts with RELA in both 4T1 and LM2 breast cancer cells endogenously (Fig. 5, A and B) and in 293T cells when expressed exogenously (fig. S6B). To determine the roles of the CECR2-RELA interaction on transcription of NF-κB–targeted genes, we performed chromatin immunoprecipitation (ChIP)–qPCR analyses of CECR2, RELA, transcriptional activation mark (H3K9/18ac), and RNA polymerase II (Pol II) at the promoters of NF-κB target genes *CSF1* and *CXCL1*. Depletion of CECR2 or RELA decreased the enrichment of H3K9/18ac and Pol II at the promoters of *CSF1* and *CXCL1* in both LM2 (Fig. 5, C and D, and fig. S6, C to E) and 4T1 cells (fig. S6, F and G). *CECR2* deletion had no effect on RELA binding to these promoters (Fig. 5, C and D, and fig. S6, C and E to G). In contrast, RELA depletion inhibited CECR2 binding (Fig. 5D and fig. S6E), suggesting that RELA recruits CECR2 to activate gene expression. Consistent with these results, RELA or CECR2 depletion decreased the expression of NF-κB target genes and metastasis-promoting genes, as well as the migration and invasion ability of LM2 cells, to a similar extent (fig. S7, A to C).

Because CECR2 is a bromodomain-containing protein and bromodomains interact with acetylated proteins, we asked whether CECR2 interacted with RELA by recognizing acetylated residues in RELA. It was previously shown that the bromodomains of bromodomain-containing 4 (BRD4) recognize lysine-310 acetylation of RELA (*44*). We found that mutation of this residue markedly decreased its interaction with CECR2 (Fig. 5E). Moreover, deletion of the bromodomain of CECR2 inhibited its interaction with RELA (Fig. 5F). These results suggest that CECR2 interacts with acetylated RELA through its bromodomain.

To further confirm the importance of RELA-CECR2 complex in regulating NF-κB target gene expression and metastasis, we reintroduced WT and lysine-310 acetylation mutant (MT) RELA into *RELA* knockout (*RELA* sg) LM2 cells and performed ChIP-qPCR analyses of CECR2, RELA, H3K9/18ac, and Pol II at the promoters of *CSF1* and *CXCL1* (fig. S7, D to F). We found that both WT and MT RELA bind to these promoters to a similar extent, which is consistent with a previous report (*45*). As expected, WT RELA strongly increased Pol II recruitment, CECR2 binding, and activation marker H3K9/18ac in *RELA* knockout cells. Although MT RELA was still able to increase Pol II recruitment, it was unable to increase CECR2 binding and H3K9/18ac. Although WT RELA had no effect on proliferation of *RELA* knockout cells, it increased their migration and invasion ability (fig. S7, G to I). In contrast, MT RELA had no effect on proliferation, migration, and invasion (fig. S7, G to I).

We then studied the function of RELA-CECR2 complex using CECR2 bromodomain–specific inhibitors, NVS-CECR2-1 and GNE-886 (*28*), which are capable of blocking the interaction between CECR2 and RELA (Fig. 5G). Both NVS-CECR2-1 and GNE-886 also reduced the expression of *CSF1/2* and *CXCL1* in a dose-dependent manner in LM2 metastatic breast cancer cells, PC9-BrM4 metastatic lung cancer cells, and YUMM1.7 melanoma cells (Fig. 5, H and I, and fig. S8, A and B). Consistently, both CECR2 inhibitors impaired the migration capability of LM2 cells by half and the invasion capability of LM2 cells by about 40%, without affecting their proliferation (Fig. 5, J and K, and fig. S8, C to F), which confirmed the prometastatic function of CECR2. These results indicate that CECR2 bromodomain is crucial for acetylated RELA to activate their target genes in multiple cancers, and pharmacological targeting of CECR2 bromodomain inhibits breast cancer migration and invasion.

CECR2 increases M2 macrophages in the tumor immune microenvironment to drive tumor metastasis

We showed that M2 macrophage ratios are increased in metastases and are correlated with CECR2 expression (Figs. 1E and 2C). Moreover, CECR2 depletion decreased the expression of genes encoding cytokines and chemokines, such as *CSF1*, *CSF2*, and *CXCL1* (Fig. 4, C and D, and fig. S5, G and H). These cytokines and chemokines are involved in the proliferation of monocytes and macrophages and their differentiation in the tumor microenvironment and breast cancer metastasis (*46*–*48*). Therefore, we investigated whether CECR2 controls metastasis by regulating the proliferation or polarization of TAMs. To examine the roles of tumor cell CECR2 on macrophage proliferation, we treated macrophages with the conditioned media (CM) from control and *Cecr2* knockout 4T1 cells. CCK8 cell proliferation assays showed that CM from control cells promoted macrophage proliferation by 2.5-fold, whereas CM from *Cecr2* knockout cells abrogated the induction of macrophage proliferation (Fig. 6A). We then examined the impact of tumor cell CECR2 on macrophage

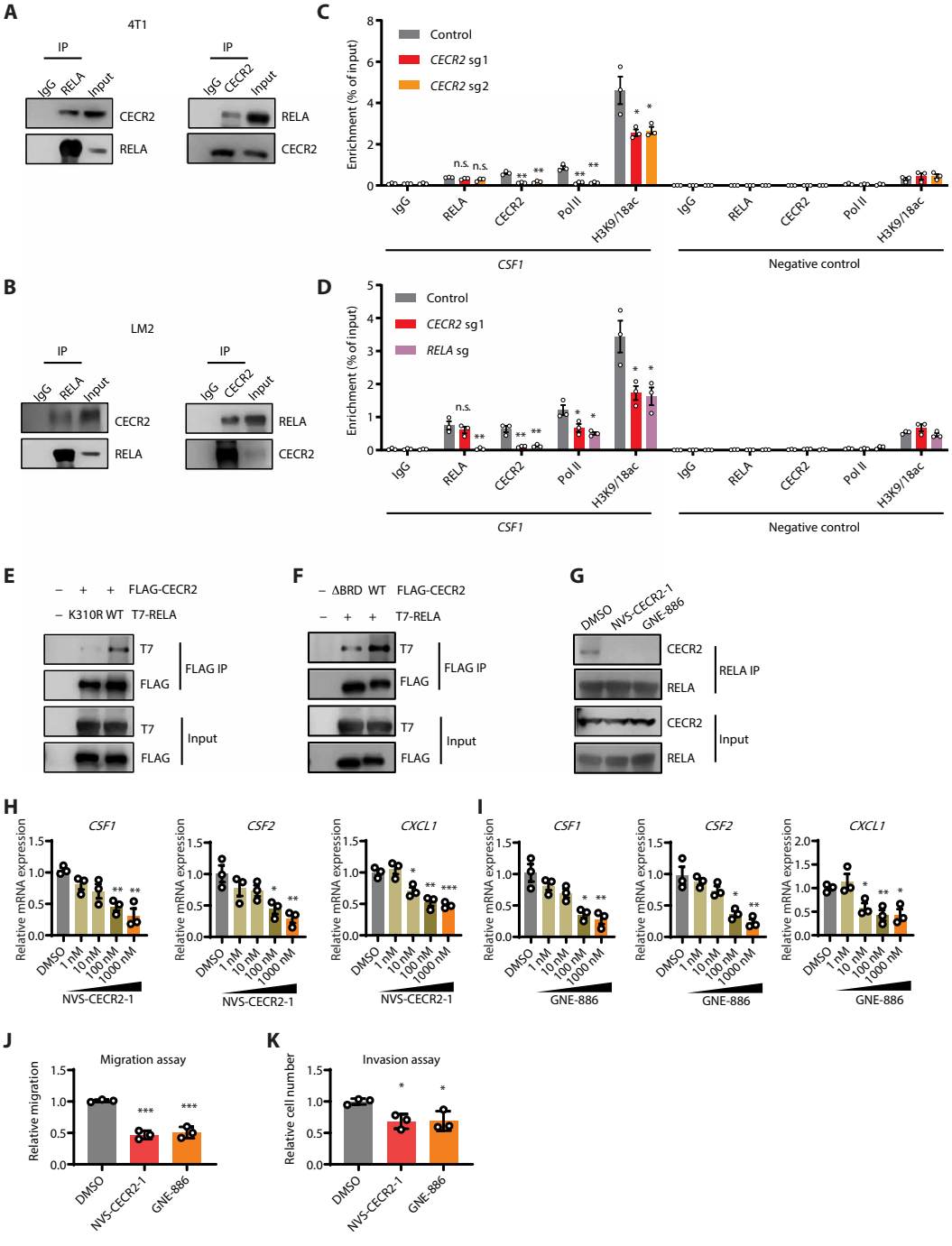

Fig. 5. CECR2 interacts with acetylated RELA using its bromodomain to activate NF-κB response genes. (**A** and **B**) Western blot analysis of cell lysates (input) and immunoprecipitates (IP) from 4T1 (A) and LM2 (B) cells stimulated with TNF-α (20 ng/ml) for 0.5 hours with the indicated antibodies. IgG, immunoglobulin G. (**C** and **D**) ChIP-qPCR analyses for the indicated proteins or histone mark at the *CSF1* promoter and a nonbinding region downstream of *CSF1* as the negative control. Control and *CECR2* knockout (*CECR2* sg1 and *CECR2* sg2) LM2 cells (C) and control, *CECR2* knockout (*CECR2* sg1), and *RELA* knockout (*RELA* sg) LM2 cells (D) were stimulated with TNF-α (20 ng/ml) for 0.5 hours. (**E**) Western blot analysis of cell lysates (Input) and anti-FLAG IP for human embryonic kidney (HEK) 293T cells transfected with the indicated combination of vectors expressing FLAG-CECR2, K310R mutated RELA, and WT RELA. (**F**) Western blot analysis of cell lysates (Input) and anti-FLAG IP for HEK293T cells transfected with the indicated combination of vectors expressing WT FLAG-CECR2, FLAG-CECR2 mutant with bromodomain deletion (ΔBRD), and T7-RELA. (**G**) Western blot analysis of cell lysates (input) and anti-RELA IP for LM2 cells pretreated with control dimethyl sulfoxide (DMSO) or CECR2 inhibitors (1 μM NVS-CECR2-1 or 1 μM GNE-886) for 2 days and then stimulated with TNF-α (20 ng/ml) for 0.5 hours. (**H** and **I**) RT-qPCR analyses of *CSF1*, *CSF2*, and *CXCL1* expression in LM2 cells pretreated with the indicated concentration of NVS-CECR2-1 (H) or GNE-886 (I) for 2 days. (**J**) Scratch migration assays comparing the closure of wound healing distance in LM2 cells treated with DMSO, 1 μM NVS-CECR2-1, or 1 μM GNE-886 for 2 days. (**K**) Transwell invasion assays comparing LM2 cells treated with DMSO, 1 μM NVS-CECR2-1, or 1 μM GNE-886 for 2 days. The *P* values of unpaired two-tailed Student's *t* test (C, D, and H to K) are shown. **P* < 0.05, ***P* < 0.01, and ****P* < 0.001. Representative data from triplicate experiments are shown, and data are presented as mean ± SEM.

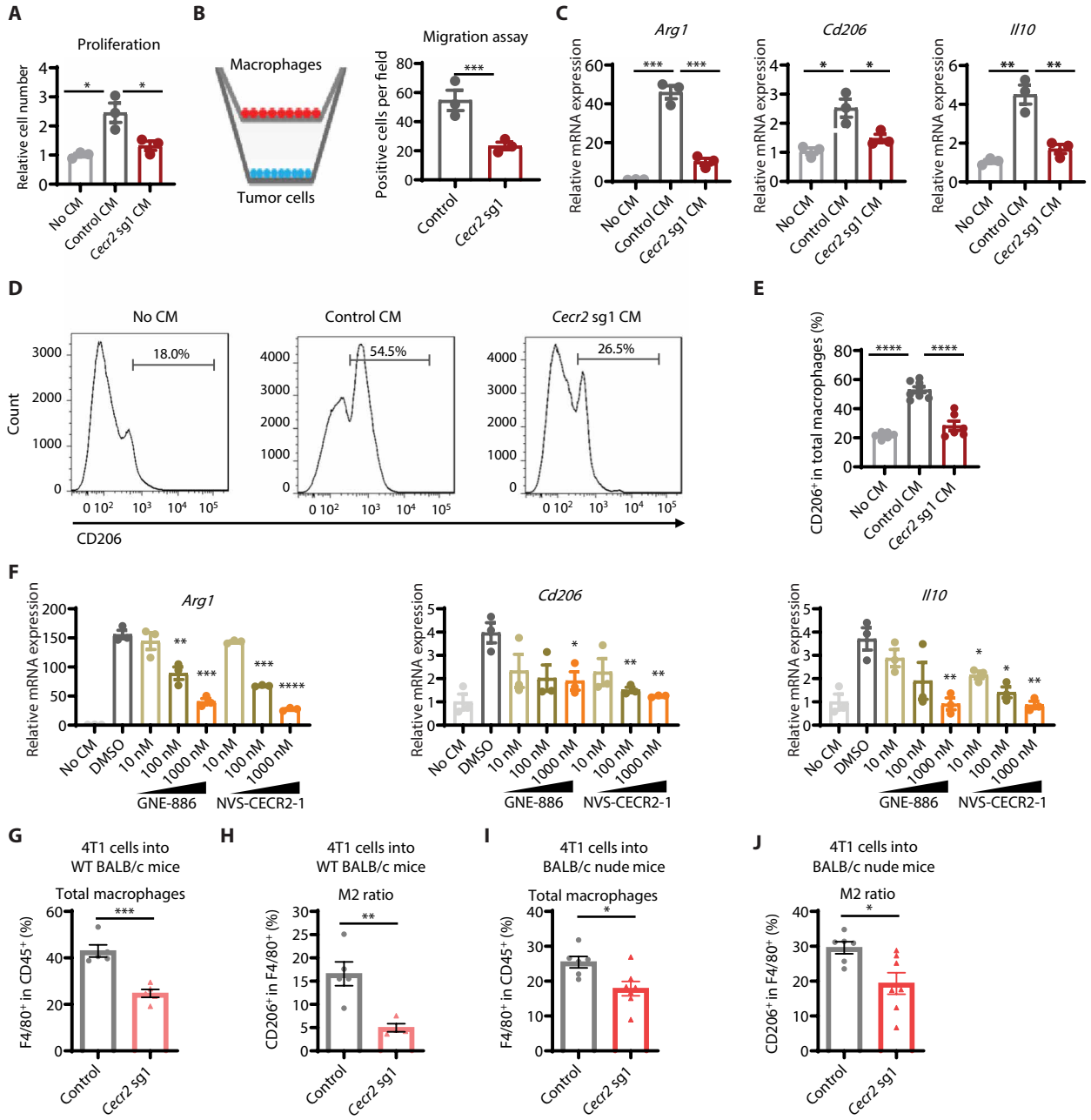

Fig. 6. CECR2 expression in breast cancer cells increases M2 macrophage proportions in tumor microenvironment. (**A**) CCK8 cell proliferation assays for macrophages cultured in RPMI 1640 medium with or without conditioned medium (CM) from control or *Cecr2* knockout 4T1 cells. (**B**) Schematics of transwell coculture experiments (left) and quantification of migrated macrophages (right). Macrophages were seeded into the top chamber (transwell size, 8 μm), and control or *Cecr2* knockout (*Cecr2* sg1) 4T1 cells were seeded into the bottom chamber. (**C**) RT-qPCR analysis for M2 markers *Arg1*, *Cd206*, and *Il10* in macrophages cultured with or without CM from control or *Cecr2* knockout 4T1 cells. (**D** and **E**) Flow cytometry analysis for the expression of the M2 marker CD206 in macrophages cultured with or without CM from control or *Cecr2* knockout 4T1 cells. Representative plots (D) and quantification of the percentage of CD206-positive cells in total macrophages (E) are shown. (**F**) RT-qPCR analyses for M2 markers *Arg1*, *Cd206*, and *Il10* in macrophages. Macrophages were seeded into a six-well plate and treated with CM harvested from 4T1 cells treated with DMSO, GNE-886, or NVS-CECR2-1 at the indicated dosage for 2 days. (**G** and **H**) Flow cytometry analysis for macrophages isolated from the lungs from immunocompetent WT BALB/c mice after tail vein injection of control ($n = 5$) or *Cecr2* knockout (sg1) 4T1 cells ($n = 5$) at week 5. The percentages of total macrophages (G) and the ratios of M2 macrophages to the total macrophages (H) are shown. (**I** and **J**) Flow cytometry analysis for macrophages isolated from the lungs from immunodeficient BALB/c nude mice after tail vein injection of control ($n = 6$) or *Cecr2* knockout (sg1) 4T1 cells ($n = 7$) at week 2. The percentages of total macrophages (I) and the ratios of M2 macrophages (J) are shown. The *P* values of unpaired two-tailed Student's *t* test (A to C and E to J) are shown. *$P < 0.05$; **$P < 0.01$; ***$P < 0.001$; ****$P < 0.0001$. Representative data from triplicate experiments are shown (A to F), and data are presented as mean ± SEM.

migration in a Boyden chamber coculture system, in which tumor cells with or without CECR2 depletion were placed into the lower chamber and macrophages were seeded into the upper chamber (Fig. 6B). We found that *Cecr2* deletion decreased macrophage migration by 2.3-fold (Fig. 6B). We next asked whether tumor cell–expressed CECR2 affected macrophage polarization by treating macrophages with CM. We found that control CM strongly induced the expression of M2 macrophage markers, whereas *Cecr2* knockout CM was defective at inducing their expression, as shown by RT-qPCR analysis of *Arg1* and *Il10* as well as RT-qPCR and flow cytometric analysis of CD206 (Fig. 6, C to E). The mRNA concentrations of genes encoding IL-4 and IL-13, two cytokines that are known to affect M2 macrophage polarization, were not changed (fig. S9A). We also did not observe a change in *Tnfa* mRNA concentrations (fig. S9A). In contrast, the mRNA concentrations of genes encoding IL-6 and transforming growth factor–β1, which could modulate M2 macrophage polarization, were down-regulated upon *CECR2* deletion in both LM2 and 4T1 cells (fig. S9, B and C).

To determine whether pharmacologically targeting CECR2 is a potential therapeutic option for metastatic breast cancer, we treated 4T1 cells with different dosages of the CECR2 bromodomain inhibitor NVS-CECR2-1 or GNE-886 and then used the CM from these cells to treat macrophages. We found that the induction of M2 macrophage markers by CM from 4T1 cells was suppressed by CECR2 inhibitor treatment in a dose-dependent manner (Fig. 6F). In contrast, treatment with NVS-CECR2-1 or GNE-886 on macrophage directly did not affect the expression of M2 macrophage markers (fig. S9D). To examine the roles of CECR2 in 4T1 cells on macrophage polarization in vivo, we first performed flow cytometry analysis of lung metastases from WT BALB/c mice implanted with 4T1 cells through the tail vein. We showed that CECR2 loss in 4T1 cells decreased the percentage of total macrophages from 44.9 to 24.1% and the ratio of M2 macrophages from 16.6 to 5%, but it had minimal effect on the ratio of M1 macrophages (Fig. 6, G and H, and fig. S10, A to C). Flow cytometry analysis of lung metastasis did not reveal changes in proportions of $CD4^+$ or $CD8^+$ T cells but showed induction of GZMB-positive cells, which implies that their tumor-killing activity increased upon CECR2 depletion (fig. S10, D to H). Consistently, CECR2 depletion in 4T1 cells caused reduction of total macrophages from 25.5 to 17.9% and the ratio of M2 macrophages from 29.6 to 19.3%, without affecting M1 macrophages or NK cells in BALB/c nude mice (Fig. 6, I and J, and fig. S10, I to K).

Colony-stimulating factor 1 (CSF1) was shown to play major roles in the regulation of macrophages (*49*, *50*). To determine whether CSF1 mediates the effects of CECR2 on macrophage and tumor growth, we overexpressed CSF1 in *Cecr2* knockout 4T1 tumor cells (fig. S11A). The 4T1 cell lines with control vectors (Control + EV), *Cecr2* knockout (Cecr2 sg1 + EV), or *Cecr2* knockout with *CSF1* overexpression (Cecr2 sg1 + *CSF1*) were injected into WT BALB/c mice through the tail vein. The metastatic ability of those cells was assayed with India ink staining of the whole lung and hematoxylin and eosin (H&E) staining of the lung sections. We found that decreased lung metastasis caused by *Cecr2* loss was mostly restored by *CSF1* overexpression (Fig. 7, A to D). Similar results were observed in BALB/c nude mice, although the extent of rescue was slightly less than that in the WT mice (fig. S11, B and C), suggesting that CSF1 promotes metastasis through both T cell–dependent and T cell–independent manner. We then examined the macrophage and activated $CD8^+$ T cell populations in lung lesions using flow cytometry assays. We found that *Cecr2* deletion in 4T1 cells decreased the percentage of macrophages from 80.2 to 52.3% and the percentage of M2 macrophages from 17.6 to 12.9%, whereas overexpression of *CSF1* suppressed these phenotypes (Fig. 7, E and F, and fig. S11, D and E). Of note, the numbers of $CD4^+$ and $CD8^+$ T cells were not changed upon *Cecr2* deletion or *CSF1* overexpression (fig. S11, F to H). However, activated $CD8^+$ T cells (GZMB positive) increased from 21 to 45.9% in lung metastases upon *Cecr2* deletion, and *CSF1* overexpression reversed this increase (Fig. 7G and fig. S11I).

To assess the therapeutic potential of CECR2-targeted therapy in vivo, WT BALB/c mice implanted with 4T1 cells by tail vein injection were treated with NVS-CECR2-1 or phosphate-buffered saline (PBS) every other day for 28 days (Fig. 7H). We found that NVS-CECR2-1 treatment strongly inhibited the ability of 4T1 cells to metastasize to the lungs (Fig. 7, I to K). We then assessed the lung metastases by flow cytometry analysis and found that NVS-CECR2-1 treatment decreased the percentage of total macrophage from 42.1 to 27.1% and M2 macrophages from 20.4 to 5.9% and increased M1 macrophages from 1.2 to 2.9% (Fig. 7, L and M, and fig. S11, J and K). Consistent with the findings from our *Cecr2* knockout and *CSF1* overexpression model, the numbers of $CD4^+$ and $CD8^+$ T cells did not change, but the number of GZMB-positive cells increased from 5.7 to 8.6% (fig. S11, L to P). Together, these results showed that targeting CECR2 inhibits macrophage polarization and breast cancer metastasis to the lungs.

DISCUSSION

In this study, we identified a druggable epigenetic factor, CECR2, that controls breast cancer metastasis. CECR2 functions through aggregated effects of multiple mechanisms in both T cell–dependent and T cell–independent manners, including promoting migration and invasion, recruiting macrophages, and inducing M2 macrophage polarization, to create an immunosuppressive microenvironment. We found that CECR2 interacts with acetylated RELA to increase chromatin accessibility and activate NF-κB targets, such as *CSF1*, *CSF2*, *CXCL1*, *TNC*, and *VEGFA*. *CECR2* depletion suppresses NF-κB response genes, which results in a decrease of total macrophages, especially M2 macrophages in tumor microenvironment, and suppression of distal metastasis. Consistently, CECR2 inhibition suppresses breast cancer metastasis by decreasing M2 macrophages and enhancing antitumor immunity (fig. S12). These results indicate that CECR2 regulates tumor immune microenvironment to promote breast cancer metastasis.

Epigenetic aberrations contribute to tumor initiation and metastasis through activating prometastatic genes and creating an immunosuppressive microenvironment (*4*, *51*–*53*). Understanding these epigenetic mechanisms is therefore essential for the development of epigenetic drugs to target both tumor cells and their immune microenvironments (*53*, *54*). We have shown that deregulation of epigenetic regulator lysine demethylase 5A (KDM5A) could promote breast cancer metastasis through increasing the expression of the metastasis-promoting gene *TNC* (*19*). Here, we found that CECR2 activates the expression of multiple prometastasis genes, including *TNC*, *VEGFA*, *IL-1B*, *IL-6*, and *MMP2*, to promote cancer cell migration and invasion. Recent studies also revealed the critical roles of epigenetic regulation on tumor immune microenvironment. For example, enhancer of zeste homolog 2 (EZH2) and DNA methyltransferase 1 (DNMT1) were shown to repress the chemokines

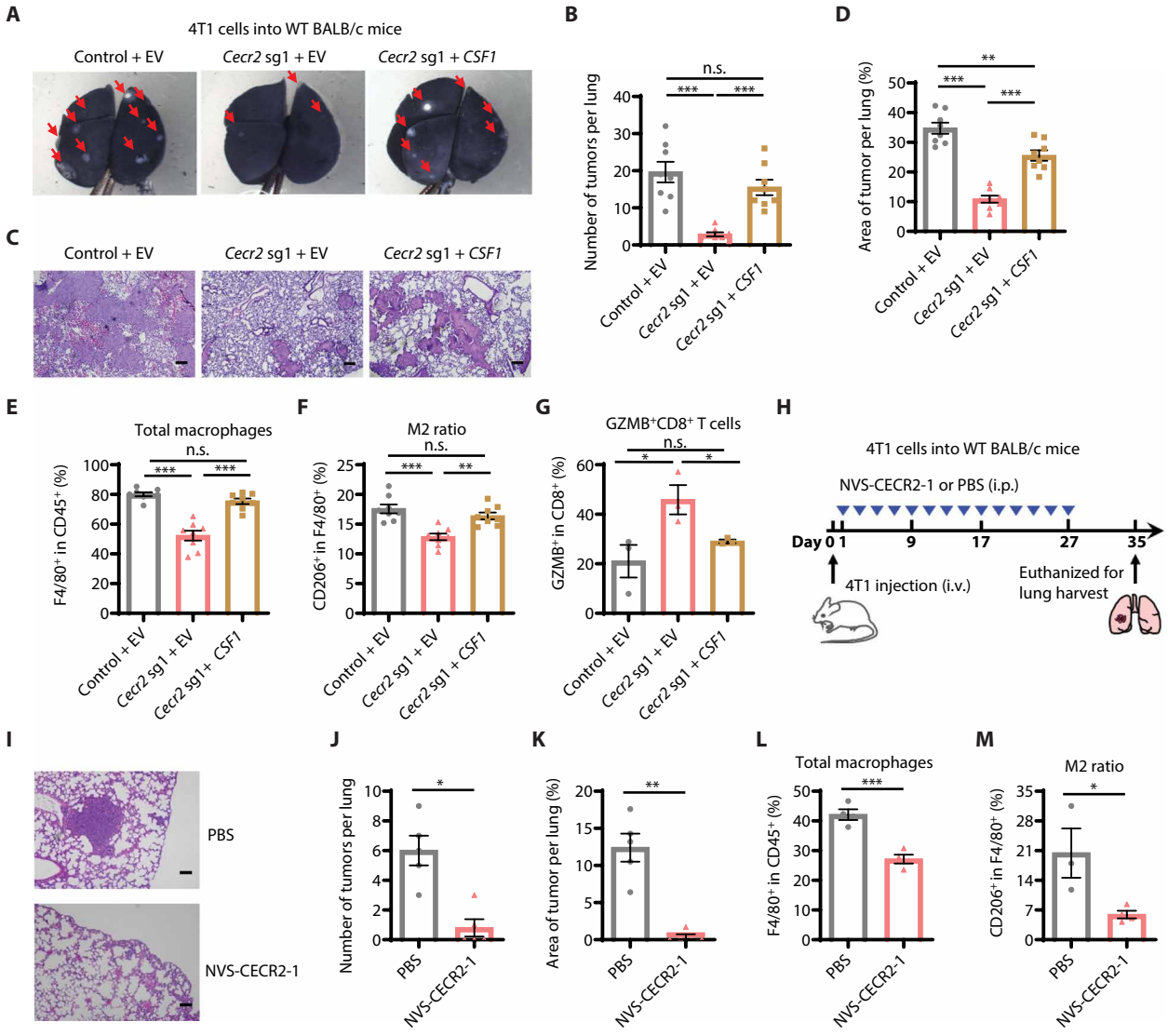

Fig. 7. CECR2 inhibition suppresses breast cancer metastasis through CSF1-mediated macrophage polarization and enhances antitumor immunity. (**A** and **B**) BALB/c WT mice were injected with control 4T1, *Cecr2* knockout (sg1) 4T1 cells, or *Cecr2* knockout 4T1 cells with *CSF1* overexpression ($n = 8$ for all the groups) through the tail vein. Metastatic lesions in the lungs at week 3 after tumor cell injection were stained by India ink. Representative images (A) and quantification of metastases in the lungs (B) are shown. Arrows indicate tumor nodules. (**C** and **D**) H&E staining of the lungs from mice in (A) at week 3. Representative images (C) and quantification of tumor areas in the lungs (D) are presented. Scale bars, 200 μm. (**E** to **G**) Flow cytometry analysis for lung lesions isolated from BALB/c WT mice injected with control 4T1, *Cecr2* knockout (sg1) 4T1 cells, or *Cecr2* knockout 4T1 cells with *CSF1* overexpression [$n = 8$ for (E) and (F) and $n = 3$ for (G)] by the tail vein at week 3. Quantification of the percentages of total macrophages ($CD45^+F4/80^+$) (E), M2 macrophages ($CD45^+F4/80^+CD206^+$) (F), and granzyme B–positive ($GZMB^+$) $CD8^+$ T cells ($CD45^+CD8^+GZMB^+$) (G) is shown. (**H**) Schematic illustration of NVS-CECR2-1 treatment. BALB/c mice were treated with intraperitoneal (i.p.) injection of NVS-CECR2-1 (10 μg per injection per mouse) or an equal volume of PBS ($n = 5$ for each group) every other day for 28 days, 1 day after tail vein injection of 4T1 cells (1×10^5 per mouse). All mice were euthanized on day 35 to collect lungs, and H&E staining was performed. i.v., intravenous. (**I** to **K**) Representative H&E staining (I), quantification of total tumor lesions per lung (J), and percentage of tumor area per lung (K) of the lungs for mice treated as described in (H). (**L** and **M**) Flow cytometry analyses for total macrophages (L) and M2 macrophage ratio (M) isolated from the lungs of BALB/c mice treated as described in (H). The *P* values calculated by unpaired two-tailed Student's *t* tests (E to G, L, and M) or Mann-Whitney tests (B, D, J, and K) are shown. $^*P < 0.05$; $^{**}P < 0.01$; $^{***}P < 0.001$. Data are presented as mean ± SEM.

CXCL9 and CXCL10, critical for T helper 1 cell trafficking to ovarian tumors (*55*). Polycomb repressive complex 2 (PRC2)–mediated epigenetic silencing in tumor cells not only plays an oncogenic role but also contributes to the decreased recruitment of $CD4^+$ and $CD8^+$ T cells into human colon cancer tissue (*56*). We previously showed that KDM5 histone demethylases contribute to the immunosuppressive microenvironment by suppressing stimulator of interferon genes (*STING*) in breast cancer (*43*). Melanoma cells overexpress H3K27 demethylase KDM6B to activate NF-κB–mediated gene expression, leading to a favorable microenvironment for melanoma growth and metastasis (*57*). Similarly, we demonstrate that the epigenetic reader CECR2 is required for metastatic breast cancer cells to express NF-κB target genes, including cytokine genes CSF1/2/3 and CXCL1. CSF1/2/3 was shown to promote the polarization and

proliferation of TAMs, in which the checkpoint proteins are triggered to suppress T cell activation (*58*–*60*). CXCL1 was previously shown to attract myeloid-derived suppressor cells (MDSCs) to suppress antitumor immunity in the tumor microenvironment (*48*, *61*). These cytokines also function in a paracrine fashion to recruit M2 TAMs (*62*), which are usually found in an immunosuppressive tumor microenvironment and support cancer cells to metastasize to distant organs (*13*, *63*). We found that CECR2 depletion reversed immune suppression at the metastatic sites in breast cancer, suggesting that CECR2 promotes an immunosuppressive microenvironment at the metastatic sites. Therefore, targeting CECR2 may suppress breast cancer metastasis by simultaneously inhibiting the expression of prometastasis genes and enhancing antitumor immunity.

Breast cancer can be classified into four subtypes by their intrinsic molecular: luminal A (resembling the histological phenotype: ER^+, PR^+, $HER2^-$, $Ki67^-$), luminal B (ER^+, PR^+, $HER^{+/-}$, $Ki67^+$), $HER2^+$ (ER^-, PR^-, $HER2^+$), and basal-like subtype (ER^-, PR^-, $HER2^-$) (*64*). The more aggressive types of breast cancer (ER^- subtypes) usually have a higher frequency of tumor-infiltrating lymphocytes than the less aggressive luminal A subtype (*65*). Here, we show that the distal metastasis samples are clustered into the low immunogenic group compared to primary tumors, regardless of their ER status. These results are consistent with our previous finding that tumor-infiltrating lymphocytes are lower in metastasis compared to primary samples (*31*). CECR2 expression was higher in metastases compared to primary tumors, regardless of the breast cancer subtypes in primary tumors. Consistently, *CECR2* expression was correlated with metastasis-free survival in all subtypes of breast cancer, as well as in gastric and ovarian cancers. Because CECR2 inhibitors suppress the expression of its target genes in metastatic breast cancer, lung cancer, and melanoma cells, our results suggest that CECR2 may be a general target for treating metastatic diseases in multiple cancer types.

We found that macrophages are the major immune cell differences in tumor microenvironment between metastases and primary breast tumor samples. We further showed that CECR2 regulates macrophages to promote breast tumor metastases. One limitation of our study is that we only classified macrophages using M1 marker CD86 and M2 marker CD206, but macrophages in tumors are more heterogeneous than these two subtypes. A recent mass cytometry analysis found multiple subtypes of macrophages, including early immigrant macrophages ($HLA\text{-}DR^{int}CD192^+$), tissue-resident macrophages ($CD206^+HLA\text{-}DR^{int}$), and TAMs ($CD64^{high}HLA\text{-}DR^{high}$) in breast tumors (*7*). Similarly, a recent single-cell RNA-seq study identified different subpopulations of macrophages based on their gene expression signature (*66*). Among these subpopulations, $SPP1^+$ and $C1QC^+$ TAMs are M2-like, whereas $ISG15^+$ TAMs are M1-like. Furthermore, coexpression of M1 and M2 gene signatures was found in macrophage subsets (*66*). However, our flow cytometry analysis found minimal macrophages that were positive for both CD86 (M1 marker) and CD206 (M2 marker). It is possible that CECR2 is involved in the regulation of specific subsets of macrophages. More detailed analysis of macrophage subsets upon perturbation of CECR2 is needed to define the roles of CECR2 in regulating the tumor microenvironment in the future. Related to this, another limitation of the current study is that we have not extensively characterized the contribution of other immune cell subsets, including T cells and MDSCs, to the roles of CECR2 in metastasis. Further understanding of these other immune cells will be needed to design appropriate treatment strategies.

Bromodomain is the acetyl-lysine "reader" module in epigenetic factors, and targeting bromodomain has been shown to promote anti-inflammatory and anticancer activities (*67*). Multiple inhibitors against bromodomain and extraterminal domain (BET) proteins are already in clinical testing (*14*). Similar to BET bromodomains, the bromodomain of CECR2 is predicted to be highly druggable (*27*). Pharmacological inhibitors of CECR2, NVS-CECR2-1 and GNE-886, have been developed. Treatment with these CECR2 inhibitors substantially suppressed the expression of CECR2 targets CSF1/2 and CXCL1 in multiple metastatic cancer cells, suggesting a possible therapeutic approach to inhibit immunosuppression in the metastatic tumor microenvironment. Our results also support testing of anti-CSF1 therapeutic antibodies (MCS110, PD-0360324) in the clinic. Together, CECR2 bromodomain inhibition is a promising therapeutic strategy to treat metastatic breast cancer. This strategy reduces the expression of prometastasis genes and immune suppression at the metastatic sites and has implications for the efficacy of immunotherapies.

MATERIALS AND METHODS

Study design

In this study, we performed RNA-seq analysis of 13 matched pairs of primary and metastatic breast tumors and assessed the expression of immuno-oncology targets and epigenetic regulators and the abundance of immune cell types using CIBERSORTx (*35*). Pearson correlation analysis was used to identify epigenetic regulators associated with changes of macrophage populations in metastases. The roles of CECR2 in gene regulation and tumorigenesis were then assessed using RNA-seq, RT-qPCR, Western blotting, coimmunoprecipitation, ChIP-qPCR, ATAC-seq, flow cytometry, immunofluorescence staining, IHC staining, histopathology analysis, colony formation assays, cell proliferation assays, migration and invasion assays, animal studies, and bioinformatic and statistical analysis. Xenograft (LM2) and syngeneic (4T1) mouse models were tested to assess the effects of CECR2 depletion and inhibition on metastasis or tumor formation. Luciferase-expressing cell lines were used for in vivo imaging to assess metastatic burden. The tumor samples from these studies are also used to assess the immune cell populations. Mice were age-, gender-, and genetic background–matched and randomized to different groups of at least three animals per group before the start of each experiment. Sample size was based on prior knowledge of the intragroup variation of tumor and metastasis growth. Blinding was not done except for the histology analysis because the information was essential for the staff to conduct the studies. No data were excluded. Potent and specific CECR2 inhibitors were used to assess the therapeutic potential of targeting CECR2 using in vitro and in vivo assays.

Statistical analysis

Normality and lognormality test (Shapiro-Wilk test) was used to test normality using GraphPad Prism 9. If data passed the normality test, comparisons between two groups were performed using an unpaired two-tailed Student's *t* test. Otherwise, comparisons between two groups were performed using an unpaired two-tailed Mann-Whitney test. Comparisons between matched data of metastasis and primary tumor samples from the sample breast cancer patient were performed using Wilcoxon signed-rank test. Mantel-Cox log-rank test was performed to calculate *P* values for Kaplan-Meier

plots. Pearson correlation coefficient and one-tailed probability P value were calculated in the correlation studies. RNA-seq and ATAC-seq data are analyzed with DESeq2 analysis of the counts and adjusted using false discovery rate. Graphs represent either group mean values ± SEM or individual values (as indicated in the figure legends). For animal experiments, each tumor graft was an independent sample. All in vitro experiments were reproduced at least three times, and all animal experiments were performed once.

SUPPLEMENTARY MATERIALS

www.science.org/doi/10.1126/scitranslmed.abf5473
Materials and Methods
Figs. S1 to S12
Tables S1 and S2
MDAR Reproducibility Checklist
Data files S1 to S18
References (*68*–*84*)

View/request a protocol for this paper from *Bio-protocol*.

REFERENCES AND NOTES

1. L. A. Torre, F. Islami, R. L. Siegel, E. M. Ward, A. Jemal, Global cancer in women: Burden and trends. *Cancer Epidemiol. Biomark. Prev.* **26**, 444–457 (2017).
2. N. Harbeck, F. Penault-Llorca, J. Cortes, M. Gnant, N. Houssami, P. Poortmans, K. Ruddy, J. Tsang, F. Cardoso, Breast cancer. *Nat. Rev. Dis. Primers* **5**, 66 (2019).
3. G. P. Gupta, J. Massague, Cancer metastasis: Building a framework. *Cell* **127**, 679–695 (2006).
4. J. F. Chen, Q. Yan, The roles of epigenetics in cancer progression and metastasis. *Biochem. J.* **478**, 3373–3393 (2021).
5. D. C. Hinshaw, L. A. Shevde, The tumor microenvironment innately modulates cancer progression. *Cancer Res.* **79**, 4557–4566 (2019).
6. A. El-Kenawi, K. Hanggi, B. Ruffell, The immune microenvironment and cancer metastasis. *Cold Spring Harb. Perspect. Med.* **10**, a037424 (2020).
7. J. Wagner, M. A. Rapsomaniki, S. Chevrier, T. Anzeneder, C. Langwieder, A. Dykgers, M. Rees, A. Ramaswamy, S. Muenst, S. D. Soysal, A. Jacobs, J. Windhager, K. Silina, M. van den Broek, K. J. Dedes, M. Rodriguez Martinez, W. P. Weber, B. Bodenmiller, A single-cell atlas of the tumor and immune ecosystem of human breast cancer. *Cell* **177**, 1330–1345.e18 (2019).
8. R. D. Leek, C. E. Lewis, R. Whitehouse, M. Greenall, J. Clarke, A. L. Harris, Association of macrophage infiltration with angiogenesis and prognosis in invasive breast carcinoma. *Cancer Res.* **56**, 4625–4629 (1996).
9. B. Z. Qian, J. Li, H. Zhang, T. Kitamura, J. Zhang, L. R. Campion, E. A. Kaiser, L. A. Snyder, J. W. Pollard, CCL2 recruits inflammatory monocytes to facilitate breast-tumour metastasis. *Nature* **475**, 222–225 (2011).
10. A. Mantovani, M. Locati, Tumor-associated macrophages as a paradigm of macrophage plasticity, diversity, and polarization. *Arterioscler. Thromb. Vasc. Biol.* **33**, 1478–1483 (2013).
11. S. K. Biswas, A. Mantovani, Orchestration of metabolism by macrophages. *Cell Metab.* **15**, 432–437 (2012).
12. L. A. Tashireva, E. V. Denisov, T. S. Gerashchenko, D. N. Pautova, M. A. Buldakov, M. V. Zavyalova, J. Kzhyshkowska, N. V. Cherdyntseva, V. M. Perelmuter, Intratumoral heterogeneity of macrophages and fibroblasts in breast cancer is associated with the morphological diversity of tumor cells and contributes to lymph node metastasis. *Immunobiology* **222**, 631–640 (2017).
13. W. Chung, H. H. Eum, H. O. Lee, K. M. Lee, H. B. Lee, K. T. Kim, H. S. Ryu, S. Kim, J. E. Lee, Y. H. Park, Z. Kan, W. Han, W. Y. Park, Single-cell RNA-seq enables comprehensive tumour and immune cell profiling in primary breast cancer. *Nat. Commun.* **8**, 15081 (2017).
14. M. Yin, Y. Guo, R. Hu, W. L. Cai, Y. Li, S. Pei, H. Sun, C. Peng, J. Li, R. Ye, Q. Yang, N. Wang, Y. Tao, X. Chen, Q. Yan, Potent BRD4 inhibitor suppresses cancer cell-macrophage interaction. *Nat. Commun.* **11**, 1833 (2020).
15. A. Mantovani, A. Sica, Macrophages, innate immunity and cancer: Balance, tolerance, and diversity. *Curr. Opin. Immunol.* **22**, 231–237 (2010).
16. B. Z. Qian, J. W. Pollard, Macrophage diversity enhances tumor progression and metastasis. *Cell* **141**, 39–51 (2010).
17. C. B. Williams, E. S. Yeh, A. C. Soloff, Tumor-associated macrophages: Unwitting accomplices in breast cancer malignancy. *NPJ Breast Cancer* **2**, 15025 (2016).
18. H. Gonzalez, C. Hagerling, Z. Werb, Roles of the immune system in cancer: From tumor initiation to metastatic progression. *Genes Dev.* **32**, 1267–1284 (2018).
19. J. Cao, Z. Liu, W. K. Cheung, M. Zhao, S. Y. Chen, S. W. Chan, C. J. Booth, D. X. Nguyen, Q. Yan, Histone demethylase RBP2 is critical for breast cancer progression and metastasis. *Cell Rep.* **6**, 868–877 (2014).
20. J. Cao, Q. Yan, Histone demethylases set the stage for cancer metastasis. *Sci. Signal.* **6**, pe15 (2013).
21. L. P. Blair, Q. Yan, Epigenetic mechanisms in commonly occurring cancers. *DNA Cell Biol.* **31** (Suppl 1), S49–S61 (2012).
22. W. L. Cai, C. B. Greer, J. F. Chen, A. Arnal-Estape, J. Cao, Q. Yan, D. X. Nguyen, Specific chromatin landscapes and transcription factors couple breast cancer subtype with metastatic relapse to lung or brain. *BMC Med. Genet.* **13**, 33 (2020).
23. M. Rodriguez-Paredes, M. Esteller, Cancer epigenetics reaches mainstream oncology. *Nat. Med.* **17**, 330–339 (2011).
24. S. K. Lee, E. J. Park, H. S. Lee, Y. S. Lee, J. Kwon, Genome-wide screen of human bromodomain-containing proteins identifies Cecr2 as a novel DNA damage response protein. *Mol. Cell* **34**, 85–91 (2012).
25. G. S. Banting, O. Barak, T. M. Ames, A. C. Burnham, M. D. Kardel, N. S. Cooch, C. E. Davidson, R. Godbout, H. E. McDermid, R. Shiekhattar, CECR2, a protein involved in neurulation, forms a novel chromatin remodeling complex with SNF2L. *Hum. Mol. Genet.* **14**, 513–524 (2005).
26. P. J. Thompson, K. A. Norton, F. H. Niri, C. E. Dawe, H. E. McDermid, CECR2 is involved in spermatogenesis and forms a complex with SNF2H in the testis. *J. Mol. Biol.* **415**, 793–806 (2012).
27. L. R. Vidler, N. Brown, S. Knapp, S. Hoelder, Druggability analysis and structural classification of bromodomain acetyl-lysine binding sites. *J. Med. Chem.* **55**, 7346–7359 (2012).
28. T. D. Crawford, J. E. Audia, S. Bellon, D. J. Burdick, A. Bommi-Reddy, A. Cote, R. T. Cummings, M. Duplessis, E. M. Flynn, M. Hewitt, H. R. Huang, H. Jayaram, Y. Jiang, S. Joshi, J. R. Kiefer, J. Murray, C. G. Nasveschuk, A. Neiss, E. Pardo, F. A. Romero, P. Sandy, R. J. Sims III, Y. Tang, A. M. Taylor, V. Tsui, J. Wang, S. Wang, Y. Wang, Z. Xu, L. Zawadzke, X. Zhu, B. K. Albrecht, S. R. Magnuson, A. G. Cochran, GNE-886: A potent and selective inhibitor of the cat eye syndrome chromosome region candidate 2 bromodomain (CECR2). *ACS Med. Chem. Lett.* **8**, 737–741 (2017).
29. S. G. Park, D. Lee, H. R. Seo, S. A. Lee, J. Kwon, Cytotoxic activity of bromodomain inhibitor NVS-CECR2-1 on human cancer cells. *Sci. Rep.* **10**, 16330 (2020).
30. B. Lim, W. A. Woodward, X. Wang, J. M. Reuben, N. T. Ueno, Inflammatory breast cancer biology: The tumour microenvironment is key. *Nat. Rev. Cancer* **18**, 485–499 (2018).
31. B. Szekely, V. Bossuyt, X. Li, V. B. Wali, G. A. Patwardhan, C. Frederick, A. Silber, T. Park, M. Harigopal, V. Pelekanou, M. Zhang, Q. Yan, D. L. Rimm, G. Bianchini, C. Hatzis, L. Pusztai, Immunological differences between primary and metastatic breast cancer. *Ann. Oncol.* **29**, 2232–2239 (2018).
32. J. McBryan, A. Fagan, D. McCartan, F. T. Bane, D. Vareslija, S. Cocchiglia, C. Byrne, J. Bolger, M. McIlroy, L. Hudson, P. Tibbitts, P. O. Gaora, A. D. Hill, L. S. Young, Transcriptomic profiling of sequential tumors from breast cancer patients provides a global view of metastatic expression changes following endocrine therapy. *Clin. Cancer Res.* **21**, 5371–5379 (2015).
33. J. Khan, P. K. Sharma, A. Mukhopadhaya, Vibrio cholerae porin OmpU mediates M1-polarization of macrophages/monocytes via TLR1/TLR2 activation. *Immunobiology* **220**, 1199–1209 (2015).
34. C. H. Lu, C. Y. Lai, D. W. Yeh, Y. L. Liu, Y. W. Su, L. C. Hsu, C. H. Chang, S. L. Catherine Jin, T. H. Chuang, Involvement of M1 macrophage polarization in endosomal toll-like receptors activated psoriatic inflammation. *Mediat. Inflamm.* **2018**, 1–14 (2018).
35. A. M. Newman, C. B. Steen, C. L. Liu, A. J. Gentles, A. A. Chaudhuri, F. Scherer, M. S. Khodadoust, M. S. Esfahani, B. A. Luca, D. Steiner, M. Diehn, A. A. Alizadeh, Determining cell type abundance and expression from bulk tissues with digital cytometry. *Nat. Biotechnol.* **37**, 773–782 (2019).
36. J. Zuber, J. Shi, E. Wang, A. R. Rappaport, H. Herrmann, E. A. Sison, D. Magoon, J. Qi, K. Blatt, M. Wunderlich, M. J. Taylor, C. Johns, A. Chicas, J. C. Mulloy, S. C. Kogan, P. Brown, P. Valent, J. E. Bradner, S. W. Lowe, C. R. Vakoc, RNAi screen identifies Brd4 as a therapeutic target in acute myeloid leukaemia. *Nature* **478**, 524–528 (2011).
37. R. Huether, L. Dong, X. Chen, G. Wu, M. Parker, L. Wei, J. Ma, M. N. Edmonson, E. K. Hedlund, M. C. Rusch, S. A. Shurtleff, H. L. Mulder, K. Boggs, B. Vadordaria, J. Cheng, D. Yergeau, G. Song, J. Becksfort, G. Lemmon, C. Weber, Z. Cai, J. Dang, M. Walsh, A. L. Gedman, Z. Faber, J. Easton, T. Gruber, R. W. Kriwacki, J. F. Partridge, L. Ding, R. K. Wilson, E. R. Mardis, C. G. Mullighan, R. J. Gilbertson, S. J. Baker, G. Zambetti, D. W. Ellison, J. Zhang, J. R. Downing, The landscape of somatic mutations in epigenetic regulators across 1,000 paediatric cancer genomes. *Nat. Commun.* **5**, 3630 (2014).
38. V. S. LeBleu, J. T. O'Connell, K. N. Gonzalez Herrera, H. Wikman, K. Pantel, M. C. Haigis, F. M. de Carvalho, A. Damascena, L. T. Domingos Chinen, R. M. Rocha, J. M. Asara, R. Kalluri, PGC-1α mediates mitochondrial biogenesis and oxidative phosphorylation in cancer cells to promote metastasis. *Nat. Cell Biol.* **16**, 992–1003 (2014).
39. A. Nagy, A. Lanczky, O. Menyhart, B. Gyorffy, Validation of miRNA prognostic power in hepatocellular carcinoma using expression data of independent datasets. *Sci. Rep.* **8**, 9227 (2018).
40. Y. Kang, P. M. Siegel, W. Shu, M. Drobnjak, S. M. Kakonen, C. Cordon-Cardo, T. A. Guise, J. Massague, A multigenic program mediating breast cancer metastasis to bone. *Cancer Cell* **3**, 537–549 (2003).

41. A. J. Minn, G. P. Gupta, P. M. Siegel, P. D. Bos, W. Shu, D. D. Giri, A. Viale, A. B. Olshen, W. L. Gerald, J. Massague, Genes that mediate breast cancer metastasis to lung. *Nature* **436**, 518–524 (2005).
42. P. D. Bos, X. H. Zhang, C. Nadal, W. Shu, R. R. Gomis, D. X. Nguyen, A. J. Minn, M. J. van de Vijver, W. L. Gerald, J. A. Foekens, J. Massague, Genes that mediate breast cancer metastasis to the brain. *Nature* **459**, 1005–1009 (2009).
43. L. Wu, J. Cao, W. L. Cai, S. M. Lang, J. R. Horton, D. J. Jansen, Z. Z. Liu, J. F. Chen, M. Zhang, B. T. Mott, K. Pohida, G. Rai, S. C. Kales, M. J. Henderson, X. Hu, A. Jadhav, D. J. Maloney, A. Simeonov, S. Zhu, A. Iwasaki, M. D. Hall, X. Cheng, G. S. Shadel, Q. Yan, KDM5 histone demethylases repress immune response via suppression of STING. *PLOS Biol.* **16**, e2006134 (2018).
44. B. Huang, X. D. Yang, M. M. Zhou, K. Ozato, L. F. Chen, Brd4 coactivates transcriptional activation of NF-kappaB via specific binding to acetylated RelA. *Mol. Cell. Biol.* **29**, 1375–1387 (2009).
45. L. F. Chen, Y. Mu, W. C. Greene, Acetylation of RelA at discrete sites regulates distinct nuclear functions of NF-kappaB. *EMBO J.* **21**, 6539–6548 (2002).
46. S. Ugel, F. De Sanctis, S. Mandruzzato, V. Bronte, Tumor-induced myeloid deviation: When myeloid-derived suppressor cells meet tumor-associated macrophages. *J. Clin. Invest.* **125**, 3365–3376 (2015).
47. N. Linde, M. Casanova-Acebes, M. S. Sosa, A. Mortha, A. Rahman, E. Farias, K. Harper, E. Tardio, I. Reyes Torres, J. Jones, J. Condeelis, M. Merad, J. A. Aguirre-Ghiso, Macrophages orchestrate breast cancer early dissemination and metastasis. *Nat. Commun.* **9**, 21 (2018).
48. S. Acharyya, T. Oskarsson, S. Vanharanta, S. Malladi, J. Kim, P. G. Morris, K. Manova-Todorova, M. Leversha, N. Hogg, V. E. Seshan, L. Norton, E. Brogi, J. Massague, A CXCL1 paracrine network links cancer chemoresistance and metastasis. *Cell* **150**, 165–178 (2012).
49. F. J. Pixley, E. R. Stanley, CSF-1 regulation of the wandering macrophage: Complexity in action. *Trends Cell Biol.* **14**, 628–638 (2004).
50. F. J. Pixley, Macrophage migration and its regulation by CSF-1. *Int. J. Cell Biol.* **2012**, 1–12 (2012).
51. J. Y. Lee, G. Kong, Roles and epigenetic regulation of epithelial-mesenchymal transition and its transcription factors in cancer initiation and progression. *Cell. Mol. Life Sci.* **73**, 4643–4660 (2016).
52. J. Cao, Q. Yan, Cancer epigenetics, tumor immunity, and immunotherapy. *Trends Cancer* **6**, 580–592 (2020).
53. M. Sylvestre, K. Tarte, D. Roulois, Epigenetic mechanisms driving tumor supportive microenvironment differentiation and function: A role in cancer therapy? *Epigenomics* **12**, 157–169 (2020).
54. M. A. Dawson, T. Kouzarides, B. J. Huntly, Targeting epigenetic readers in cancer. *N. Engl. J. Med.* **367**, 647–657 (2012).
55. D. Peng, I. Kryczek, N. Nagarsheth, L. Zhao, S. Wei, W. Wang, Y. Sun, E. Zhao, L. Vatan, W. Szeliga, J. Kotarski, R. Tarkowski, Y. Dou, K. Cho, S. Hensley-Alford, A. Munkarah, R. Liu, W. Zou, Epigenetic silencing of TH1-type chemokines shapes tumour immunity and immunotherapy. *Nature* **527**, 249–253 (2015).
56. N. Nagarsheth, D. Peng, I. Kryczek, K. Wu, W. Li, E. Zhao, L. Zhao, S. Wei, T. Frankel, L. Vatan, W. Szeliga, Y. Dou, S. Owens, V. Marquez, K. Tao, E. Huang, G. Wang, W. Zou, PRC2 epigenetically silences Th1-type chemokines to suppress effector T-cell trafficking in colon cancer. *Cancer Res.* **76**, 275–282 (2016).
57. W. Y. Park, B. J. Hong, J. Lee, C. Choi, M. Y. Kim, H3K27 demethylase JMJD3 employs the NF-κB and BMP signaling pathways to modulate the tumor microenvironment and promote melanoma progression and metastasis. *Cancer Res.* **76**, 161–170 (2016).
58. A. Mantovani, F. Marchesi, A. Malesci, L. Laghi, P. Allavena, Tumour-associated macrophages as treatment targets in oncology. *Nat. Rev. Clin. Oncol.* **14**, 399–416 (2017).
59. M. Hollmen, S. Karaman, S. Schwager, A. Lisibach, A. J. Christiansen, M. Maksimow, Z. Varga, S. Jalkanen, M. Detmar, G-CSF regulates macrophage phenotype and associates with poor overall survival in human triple-negative breast cancer. *Onco. Targets Ther.* **5**, e1115177 (2016).
60. E. Sami, B. T. Paul, J. A. Koziol, W. M. ElShamy, The immunosuppressive microenvironment in BRCA1-IRIS-overexpressing TNBC tumors is induced by bidirectional interaction with tumor-associated macrophages. *Cancer Res.* **80**, 1102–1117 (2020).
61. D. Wang, H. Sun, J. Wei, B. Cen, R. N. DuBois, CXCL1 is critical for premetastatic niche formation and metastasis in colorectal cancer. *Cancer Res.* **77**, 3655–3665 (2017).
62. E. Y. Lin, A. V. Nguyen, R. G. Russell, J. W. Pollard, Colony-stimulating factor 1 promotes progression of mammary tumors to malignancy. *J. Exp. Med.* **193**, 727–740 (2001).
63. J. Y. Wu, T. W. Huang, Y. T. Hsieh, Y. F. Wang, C. C. Yen, G. L. Lee, C. C. Yeh, Y. J. Peng, Y. Y. Kuo, H. T. Wen, H. C. Lin, C. W. Hsiao, K. K. Wu, H. J. Kung, Y. J. Hsu, C. C. Kuo, Cancer-derived succinate promotes macrophage polarization and cancer metastasis via succinate receptor. *Mol. Cell* **77**, 213–227.e5 (2020).
64. D. Hammerl, M. Smid, A. M. Timmermans, S. Sleijfer, J. W. M. Martens, R. Debets, Breast cancer genomics and immuno-oncological markers to guide immune therapies. *Semin. Cancer Biol.* **52**, 178–188 (2018).
65. M. Miyan, J. Schmidt-Mende, R. Kiessling, I. Poschke, J. de Boniface, Differential tumor infiltration by T-cells characterizes intrinsic molecular subtypes in breast cancer. *J. Transl. Med.* **14**, 227 (2016).
66. S. Cheng, Z. Li, R. Gao, B. Xing, Y. Gao, Y. Yang, S. Qin, L. Zhang, H. Ouyang, P. Du, L. Jiang, B. Zhang, Y. Yang, X. Wang, X. Ren, J. X. Bei, X. Hu, Z. Bu, J. Ji, Z. Zhang, A pan-cancer single-cell transcriptional atlas of tumor infiltrating myeloid cells. *Cell* **184**, 792–809.e23 (2021).
67. A. G. Cochran, A. R. Conery, R. J. Sims III, Bromodomains: A new target class for drug development. *Nat. Rev. Drug Discov.* **18**, 609–628 (2019).
68. J. Cao, L. Wu, S. M. Zhang, M. Lu, W. K. Cheung, W. Cai, M. Gale, Q. Xu, Q. Yan, An easy and efficient inducible CRISPR/Cas9 platform with improved specificity for multiple gene targeting. *Nucleic Acids Res.* **44**, e149 (2016).
69. M. Gale, J. Sayegh, J. Cao, M. Norcia, P. Gareiss, D. Hoyer, J. S. Merkel, Q. Yan, Screen-identified selective inhibitor of lysine demethylase 5A blocks cancer cell growth and drug resistance. *Oncotarget* **7**, 39931–39944 (2016).
70. R. J. Klose, Y. Zhang, Histone H3 Arg2 methylation provides alternative directions for COMPASS. *Nat. Struct. Mol. Biol.* **14**, 1058–1060 (2007).
71. B. Langmead, S. L. Salzberg, Fast gapped-read alignment with Bowtie 2. *Nat. Methods* **9**, 357–359 (2012).
72. J. Harrow, A. Frankish, J. M. Gonzalez, E. Tapanari, M. Diekhans, F. Kokocinski, B. L. Aken, D. Barrell, A. Zadissa, S. Searle, I. Barnes, A. Bignell, V. Boychenko, T. Hunt, M. Kay, G. Mukherjee, J. Rajan, G. Despacio-Reyes, G. Saunders, C. Steward, R. Harte, M. Lin, C. Howald, A. Tanzer, T. Derrien, J. Chrast, N. Walters, S. Balasubramanian, B. Pei, M. Tress, J. M. Rodriguez, I. Ezkurdia, J. van Baren, M. Brent, D. Haussler, M. Kellis, A. Valencia, A. Reymond, M. Gerstein, R. Guigo, T. J. Hubbard, GENCODE: The reference human genome annotation for The ENCODE Project. *Genome Res.* **22**, 1760–1774 (2012).
73. Y. Liao, G. K. Smyth, W. Shi, featureCounts: An efficient general purpose program for assigning sequence reads to genomic features. *Bioinformatics* **30**, 923–930 (2014).
74. M. I. Love, W. Huber, S. Anders, Moderated estimation of fold change and dispersion for RNA-seq data with DESeq2. *Genome Biol.* **15**, 550 (2014).
75. W. E. Johnson, C. Li, A. Rabinovic, Adjusting batch effects in microarray expression data using empirical Bayes methods. *Biostatistics* **8**, 118–127 (2007).
76. R. L. Barter, B. Yu, Superheat: An R package for creating beautiful and extendable heatmaps for visualizing complex data. *J. Comput. Graph. Stat.* **27**, 910–922 (2018).
77. A. Subramanian, P. Tamayo, V. K. Mootha, S. Mukherjee, B. L. Ebert, M. A. Gillette, A. Paulovich, S. L. Pomeroy, T. R. Golub, E. S. Lander, J. P. Mesirov, Gene set enrichment analysis: A knowledge-based approach for interpreting genome-wide expression profiles. *Proc. Natl. Acad. Sci. U.S.A.* **102**, 15545–15550 (2005).
78. S. M. Zhang, W. L. Cai, X. Liu, D. Thakral, J. Luo, L. H. Chan, M. K. McGeary, E. Song, K. R. M. Blenman, G. Micevic, S. Jessel, Y. Zhang, M. Yin, C. J. Booth, L. B. Jilaveanu, W. Damsky, M. Sznol, H. M. Kluger, A. Iwasaki, M. W. Bosenberg, Q. Yan, KDM5B promotes immune evasion by recruiting SETDB1 to silence retroelements. *Nature* **598**, 682–687 (2021).
79. J. Wei, M. M. Alfajaro, P. C. DeWeirdt, R. E. Hanna, W. J. Lu-Culligan, W. L. Cai, M. S. Strine, S. M. Zhang, V. R. Graziano, C. O. Schmitz, J. S. Chen, M. C. Mankowski, R. B. Filler, N. G. Ravindra, V. Gasque, F. J. de Miguel, A. Patil, H. Chen, K. Y. Oguntuyo, L. Abriola, Y. V. Surovtseva, R. C. Orchard, B. Lee, B. D. Lindenbach, K. Politi, D. van Dijk, C. Kadoch, M. D. Simon, Q. Yan, J. G. Doench, C. B. Wilen, Genome-wide CRISPR screens reveal host factors critical for SARS-CoV-2 infection. *Cell* **184**, 76–91.e13 (2021).
80. A. M. Bolger, M. Lohse, B. Usadel, Trimmomatic: A flexible trimmer for Illumina sequence data. *Bioinformatics* **30**, 2114–2120 (2014).
81. H. Li, B. Handsaker, A. Wysoker, T. Fennell, J. Ruan, N. Homer, G. Marth, G. Abecasis, R. Durbin, S. Genome, The sequence alignment/map format and SAMtools. *Bioinformatics* **25**, 2078–2079 (2009).
82. Y. Zhang, T. Liu, C. A. Meyer, J. Eeckhoute, D. S. Johnson, B. E. Bernstein, C. Nusbaum, R. M. Myers, M. Brown, W. Li, X. S. Liu, Model-based analysis of ChIP-Seq (MACS). *Genome Biol.* **9**, R137 (2008).
83. F. Ramirez, D. P. Ryan, B. Gruning, V. Bhardwaj, F. Kilpert, A. S. Richter, S. Heyne, F. Dundar, T. Manke, deepTools2: A next generation web server for deep-sequencing data analysis. *Nucleic Acids Res.* **44**, W160–W165 (2016).
84. J. T. Robinson, H. Thorvaldsdottir, W. Winckler, M. Guttman, E. S. Lander, G. Getz, J. P. Mesirov, Integrative genomics viewer. *Nat. Biotechnol.* **29**, 24–26 (2011).

Acknowledgments: We would like to thank all members of Yan, Stern, and Nguyen laboratories at Yale University for helpful discussions; L. Charette and Y. Bai at Yale Pathology Tissue Services for building TMA; C. Booth at Yale Department of Comparative Medicine for help on histological analysis; M. Zhong at Yale Stem Cell Center Genomics Core facility for help with sample preparation for RNA-seq; J. Massagué at Memorial Sloan Kettering Cancer Center for providing MDA-MB-231, LM2, and 4T1 cells; Y. Kang at Princeton University for providing BrM2 cells; D. Nguyen for providing PC9-BrM4 cells; M. Bosenberg for providing YUMM1. 7 cells; A. Cochran at Genentech for providing GNE-886; and N. Wajapeyee at the University of

Alabama Birmingham and M. Schapira at the SGC for helping with compiling the epigenetic gene list. Sequencing done at Yale Stem Cell Center Genomics Core facility was supported by the Connecticut Regenerative Medicine Research Fund and the Li Ka Shing Foundation. **Funding:** The research in this manuscript is supported by the Department of Defense Breast Cancer Research Program Awards W81XWH-15-1-0117 and W81XWH-21-1-0411 (to Q.Y.), NIH grant R21CA191548 (to Q.Y.), NIH grant P30CA016359 (to the Yale Comprehensive Cancer Center), Yale Cancer Center Class of '61 Cancer Research Award (to Q.Y.), and the James Hudson Brown-Alexander Brown Coxe Postdoctoral Fellowship (to M.Z.). **Author contributions:** M.Z., M.Y., and Q.Y. designed the research. Q.Y. conceived and oversaw the project. M.Z. performed most of the experiments. Z.Z.L., W.L.C., and M.Z. performed the bioinformatic analysis. M.Z., K.A., H.S., T.X., J.F.C., A.A., Z.T., Y.L., and M.Y. performed animal studies. M.Y., H.S., T.X., Y.Z., X. Che, and M.Z. performed in vitro assays related to macrophages. M.Z., K.A., and M.Y. performed histological analyses. L.H.C. cloned FLAG-CECR2 and DOX-inducible RELA constructs. Y.A. and S.M.L. performed some cell culture work. M.Z., M.Y., H.S., and T.X. performed flow cytometry analysis. S.J.R., V.B., J.S.M., L.P., and D.L.R. provided clinical samples, collected clinical information, and helped with experimental design related to clinical samples. M.Z., Z.Z.L., K.A., X. Chen, M.Y., and Q.Y. analyzed the data. M.Z., M.Y., and Q.Y. wrote the paper. **Competing interests:** The authors declare that they have no competing interests. **Data and materials availability:** All data associated with this study are present in the paper or the Supplementary Materials. Raw data with individual data values are in data file S18. RNA-seq data and ATAC-seq data have been deposited into the National Center for Biotechnology Information (NCBI) Gene Expression Omnibus database under GSE148005 and GSE185647, respectively. All custom codes used for data analysis are available at Zenodo (DOI 10.5281/zenodo.5797228). All noncommercially available new materials, including constructs and cell lines, that Yale has the right to provide will be made available to nonprofit or academic requesters upon completion of a standard material transfer agreement. Requests for materials may be made by contacting Q.Y. (qin.yan@yale.edu).

Submitted 5 November 2020
Resubmitted 26 October 2021
Accepted 22 December 2021
Published 2 February 2022
10.1126/scitranslmed.abf5473